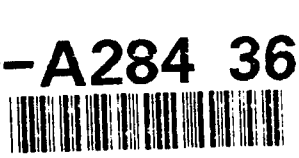

(1)

ARMY RESEARCH LABORATORY

Design of Advanced Steels for Armor Applications

Gregory B. Olson and Timothy A. Stephenson

ARL-CR-175 August 1994

Prepared by
Northwestern University
Evanston, IL

under contract
DAAL04-91-C-0073

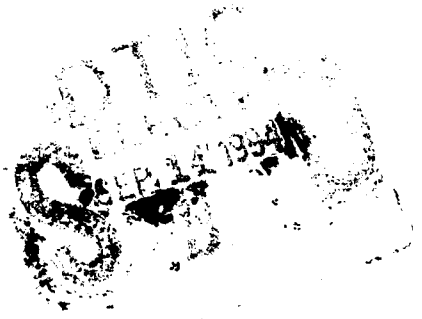

The findings in this report are not to be construed as an official Department of the Army position unless so designated by other authorized documents.

Citation of manufacturer's or trade names does not constitute an official endorsement or approval of the use thereof.

Destroy this report when it is no longer needed. Do not return it to the originator.

REPORT DOCUMENTATION PAGE

Form Approved
OMB No. 0704-0188

1. AGENCY USE ONLY *(Leave blank)*	2. REPORT DATE	3. REPORT TYPE AND DATES COVERED
	August 1994	Final Report 8/30/91-7/30/93

4. TITLE AND SUBTITLE
Design of Advanced Steels for Armor Applications

5. FUNDING NUMBERS
Contract No.
DAAL04-91-C-0073

6. AUTHOR(S)
Gregory B. Olson and Timothy A. Stephenson

7. PERFORMING ORGANIZATION NAME(S) AND ADDRESS(ES)
Northwestern University
Evanston, IL

8. PERFORMING ORGANIZATION REPORT NUMBER

9. SPONSORING/MONITORING AGENCY NAME(S) AND ADDRESS(ES)
U.S. Army Research Laboratory
Watertown, MA 02172-0001
ATTN: AMSRL-OP-PR-WT

10. SPONSORING/MONITORING AGENCY REPORT NUMBER
ARL-CR-175

11. SUPPLEMENTARY NOTES
Morris Azrin COR

12a. DISTRIBUTION/AVAILABILITY STATEMENT
Approved for public release; distribution unlimited.

12b. DISTRIBUTION CODE

13. ABSTRACT *(Maximum 200 words)*
(See reverse, page ii.)

14. SUBJECT TERMS
Armor steels, Secondary hardening steels, Fracture toughness

15. NUMBER OF PAGES
47

16. PRICE CODE

17. SECURITY CLASSIFICATION OF REPORT	18. SECURITY CLASSIFICATION OF THIS PAGE	19. SECURITY CLASSIFICATION OF ABSTRACT	20. LIMITATION OF ABSTRACT
Unclassified	Unclassified	Unclassified	UL

13. ABSTRACT

An interdisciplinary research effort has addressed the fundamental principles for the design of fracture-tough, stress-corrosion resistant, ultrahigh-strength martensitic steels for advanced armor applications. Three alloy compositions, designated MTL1, MTL2, and MTL3 were derived from thermodynamics-based computer-aided design using the THERMOCALC thermochemical database and software system. Hardness and K_{IC} fracture toughness were measured as a function of solution treatment temperature and tempering time at 482°C, and undissolved carbides were examined by analytical electron microscopy. Although the as-received carbon contents for alloys MTL2 and MTL3 exceeded the design carbon content by .03 wt. pct., optimum heat treatment for alloy MTL2 produced R_C 56.2 with 69.4 ksi$\sqrt{in}$ toughness, and R_C56.4 with 66.3 ksi$\sqrt{in}$ for MTL3. The carbon content of MTL1 fell short by .06 wt. pct., producing a hardness of R_C 55.2 at 82.2 ksi$\sqrt{in}$. Despite the low carbon content, the hardness achieved in the latter case demonstrates the effectiveness of small V additions in enhancing strength in these alloys. Ballistic testing is recommended. Based on the prototype alloy evaluations, iterative design calculations predict improved compositions. Further toughness enhancement should be achievable with a carbon content of 0.25 wt. pct., and by exploitation of multistep tempering treatments to achieve transformation toughening.

TABLE OF CONTENTS

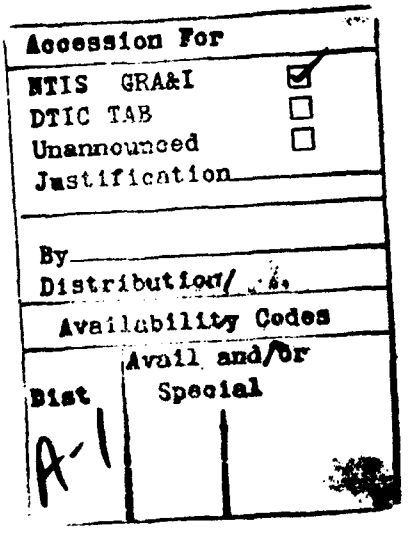

INTRODUCTION

A one-year research effort has applied principles from interdisciplinary fundamental research under the multi-institutional Steel Research Group (SRG) program toward the conceptual design of advanced armor steels. Evaluation of three initial prototype alloys has tested model predictions. Heat treatment optimization of the prototypes has demonstrated properties worthy of ballistic testing, and provided input for a second series of design calculations for improved compositions.

ALLOY DESIGN

This program has addressed improving the fracture toughness of ultrahigh strength (UHS) steels while maintaining a usable hardness level of approximately R_C 57. Property objectives are compared with existing alloys in Figure 1. Our approach to enhancing fracture toughness in these martensitic steels included (1) transformation toughening from controlled stability dispersed austenite precipitated during tempering, (2) optimization of grain-refining dispersions for resistance to microvoid nucleation, and (3) controlling the M_2C carbide precipitation strengthening to eliminate competing phases and achieve the required strength level at minimum carbon content.

Although the design approach consists of balancing and optimizing a number of quantities, it can be divided into two basic areas. The first concerns the determination of the most appropriate combination of Ni and Co to optimize three variables: the martensitic transformation temperature (M_S), the stability of precipitated austenite, and a toughening efficiency parameter. The second concerns the identity and combination of carbide formers to optimize the following variables: amount of carbide formers required to completely dissolve cementite, the driving force for precipitation, the carbide

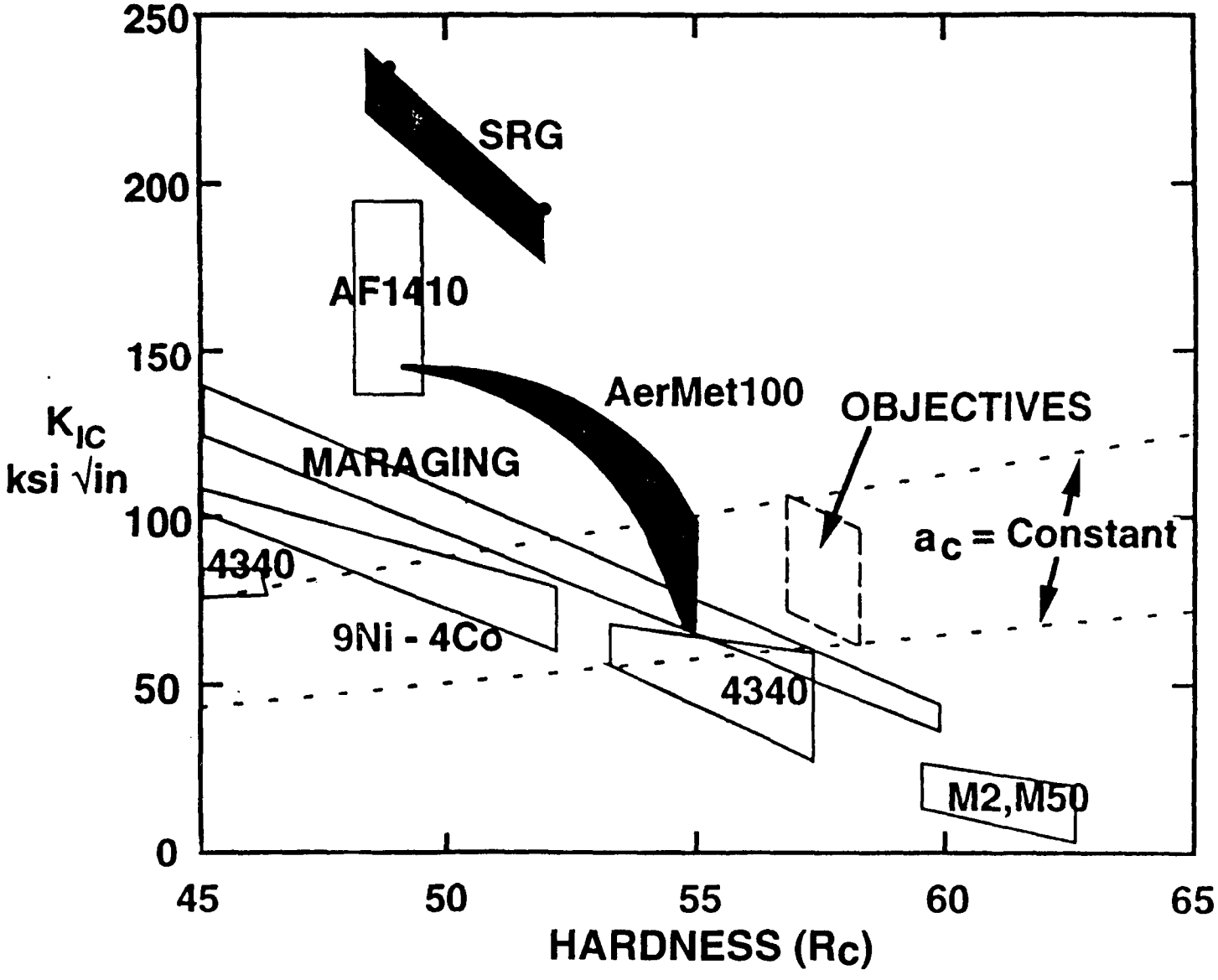

Figure 1. K_{IC} toughness vs. R_c hardness of UHS martensitic steels. Dark bands represent (a) SRG improvement of AF1410 by transformation toughening and (b) Aermet100 alloy developed by Carpenter Steel.

coarsening rate constant, and solution treatment temperature. The starting composition for these calculations was a higher carbon modification of Aermet 100 (Carpenter Steel), Fe-13.5Co-11Ni-3Cr-1.1Mo-0.27C.

Using the THERMOCALC thermochemical database and software system and a newly developed martensite kinetic model[1], an M_S contour plot was created as shown in Figure 2. The M_S temperature of Aermet 100, 244°C, was used as a target for our design and is drawn in the figure in bold.

Improved toughness can be obtained by the strain-induced transformation of metastable austenite at a crack tip[2]. This transformation-toughening mechanism can be exploited by controlling the stability of precipitated austenite formed during tempering. This stability is controlled primarily by the matrix content of Fe, Ni, and Co. The optimum stability of austenite for a given composition can be theoretically determined by computing the critical driving force required to transform an austenite particle to martensite. Figure 3 is a contour plot for the computed chemical driving force of the austenite to martensite transformation at room temperature for austenite precipitated at 500°C. This driving force is then used to determine the stability of the precipitated austenite as a function of the Ni-Co compositions. The desired austenite stability for the new alloy is that of Aermet 100 plus a factor, $\Delta(\Delta g)$, which compensates for the desired higher strength level at our R_C 57 regime. The $\Delta(\Delta g)$ parameter was calculated using a model developed by Haidemenopoulos[2], and found to equal 235 J/mole. The Δg for the Aermet 100 composition was found to be 1903.7 J/mole. Therefore, the optimum stability of the precipitated austenite for the new alloy was chosen to be the sum, 2138.7 J/mole. This contour is highlighted in bold in Figure 3. The stability increases with Co and Ni content.

An additional benefit of achieving a fine dispersion of metastable austenite is the effect of transformation dilatation on toughness. Experimental results have shown that there is a positive dependence of transformation toughening efficiency on the volume

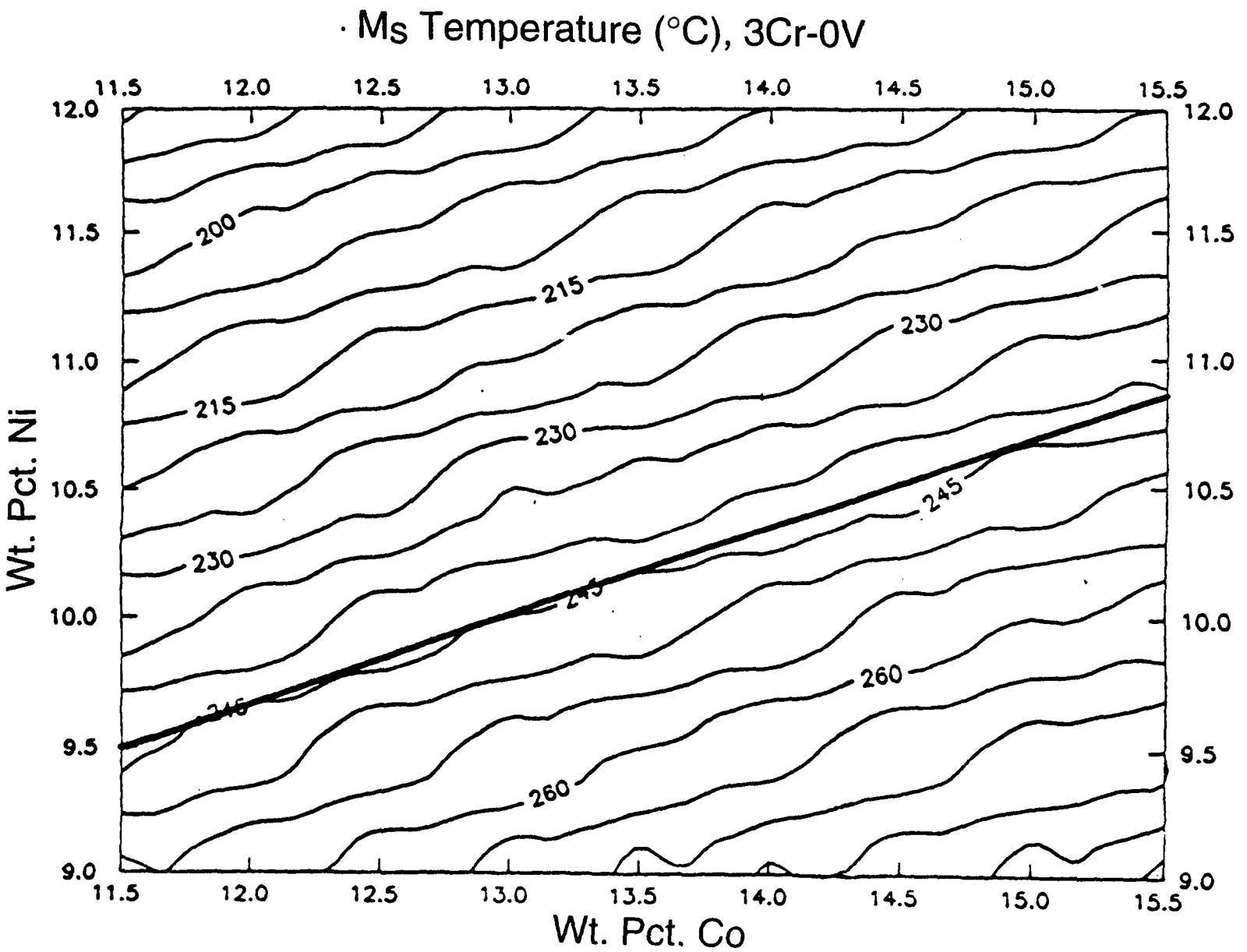

Figure 2. Computed M_S temperature contours vs. Ni and Co content for Fe-3Cr-1.1Mo-0.27C steels.

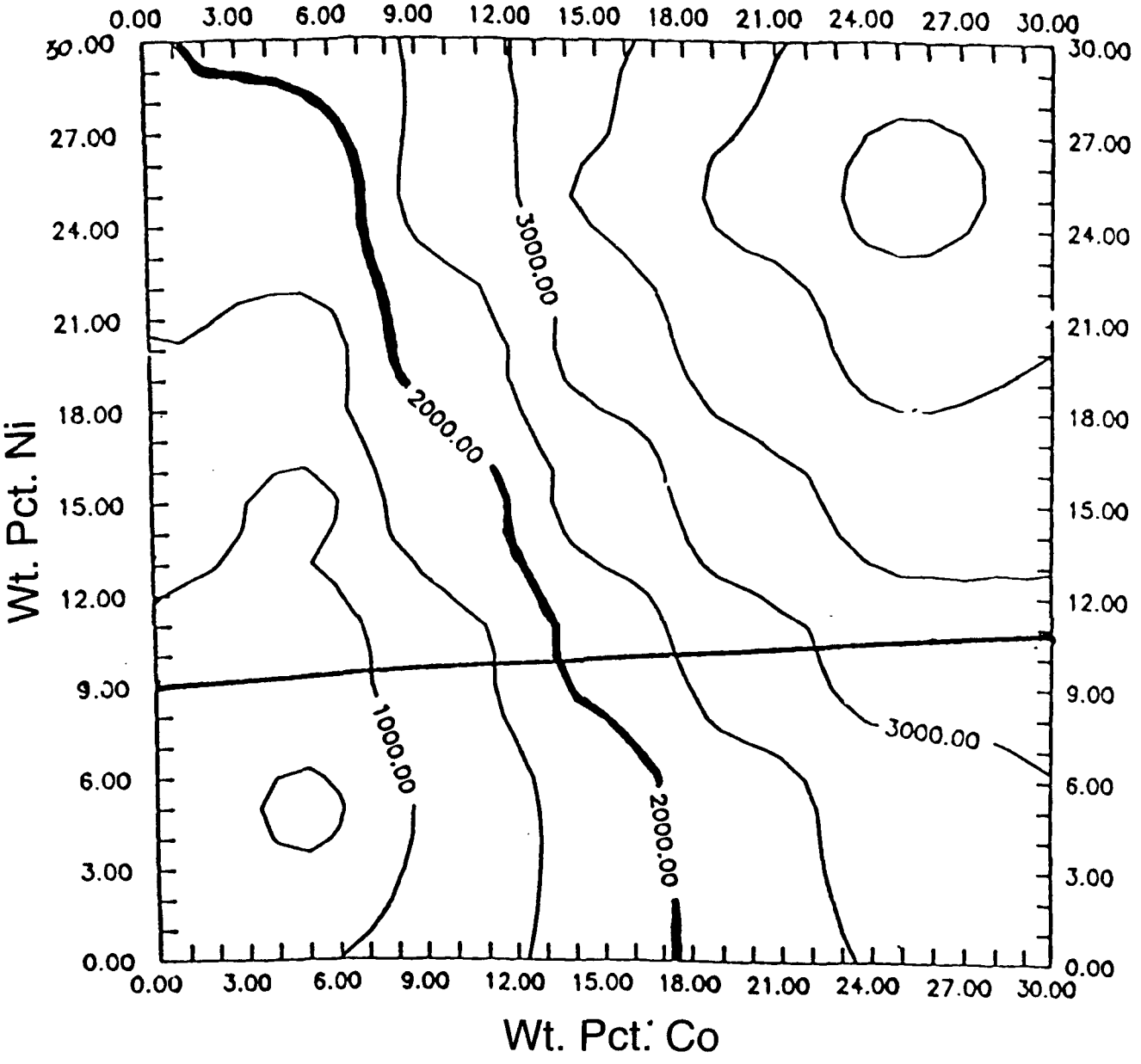

Figure 3. Computed contours of precipitated austenite stability represented by martensitic transformation driving force at room temperature (J/mole).

change to the third power[3]. We therefore define a toughening efficiency parameter (TEP) as the product of two quantities:

$$TEP = f^{\gamma} \times (\Delta V/V)^3$$

f^{γ} = the volume fraction of precipitated metastable austenite.

$\Delta V/V$ = volume change

A model for the composition dependence of $\Delta V/V$ has been developed by Kuehmann[4] for compositions containing Fe, Ni, Cr, and Co and has been employed to predict the TEP. Figure 4 is a contour plot of TEP versus weight percent Ni and Co. Three compositions were chosen by cross-referencing Figures 2, 3, and 4. The M_S temperature contour representing the 244°C line in Figure 2 was compared to the austenite stability diagram, Figure 3, where the 2,138 J/mole isopleth was identified. These two lines were transferred to the toughening diagram, Figure 4. Using these variables as guidelines, the most appropriate Ni-Co composition was chosen, 13.5Co-10.6Ni (henceforth referred to as MTL2). Two other constant M_S compositions were chosen +/- 1 wt. pct. Co on either side of the primary composition, alloy MTL1 at 12.5Co-10.2Ni and alloy MTL3 at 14.5Co-10.9Ni. These compositions are marked on Figure 4.

The second area of the design concerns optimization of the carbide formers. The precipitation of metastable coherent M_2C carbide from ferrite improves strength via secondary hardening and improves toughness by dissolution of metastable cementite[3]. However, precipitation of M_2C must be completed without the nucleation of more stable carbides, (M_6C, $M_{23}C_6$, and M_7C_3) which will decrease toughness[3]. Completion of the reaction $2M+C \rightarrow M_2C$ is required to dissolve all of the transient Fe_3C carbides. Thus, the mole fraction of the carbide formers must be at least equal to twice the mole fraction of carbon, i.e. $X_{Mo}+X_{Cr}+X_V > 2X_C$. In addition, it is important to minimize the final carbide size in order to maximize the strength. The final carbide size is determined by the initial critical nucleus size which is inversely related to the precipitation thermodynamic driving force as described by the Langer-Schwartz theory of precipitation

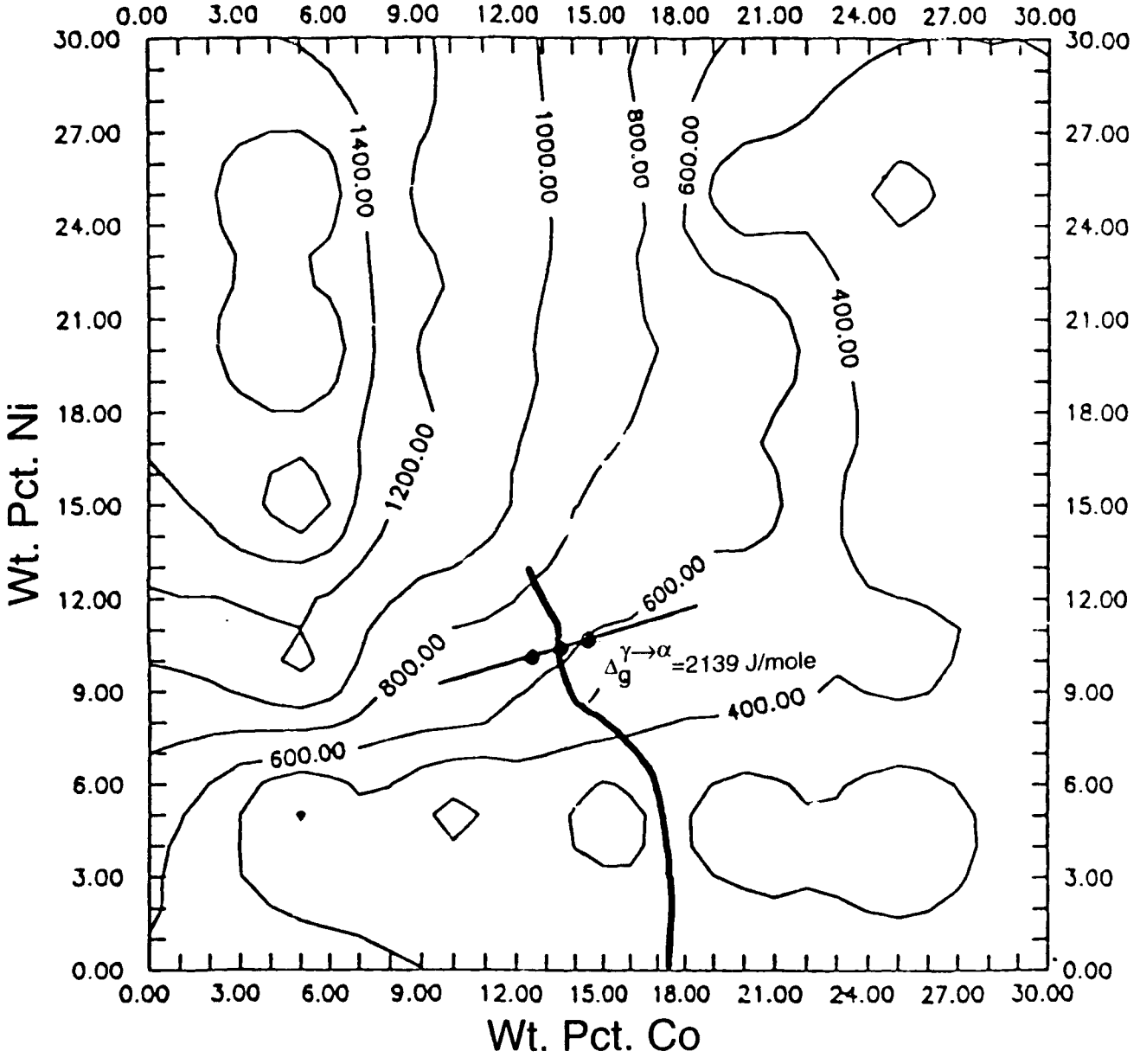

Figure 4. Computed contours of toughening efficiency parameter (TEP) vs. Ni and Co content. Contour of desired austenite stability is superimposed from Fig. 3.

from highly supersaturated solid solutions[5]. Thus, to minimize the final carbide size the precipitation driving force must be maximized. Included with this optimization is the coarsening rate constant which influences the overall rate of precipitation of the carbides. It is desirable to maximize this parameter by designing the kinetic competition so that carbide precipitation can be driven to completion before impurity segregation to the grain boundaries can occur. Finally, it is important to limit the content of carbide formers to maintain an acceptable solution temperature.

Our previous work has demonstrated a beneficial effect of V in enhancing the M_2C precipitation driving force[3]. Looking initially at the effect of such V addition, we balance the competing benefits and trade-offs of the solution temperature, precipitation driving force, and the coarsening rate constant K_C. Figure 5 illustrates a phase diagram section for alloy MTL2 for 0 to 1 wt. pct. V addition. This diagram remains essentially unchanged for alloys MTL1 and MTL3. The temperature required to put all components into solution in austenite rises sharply with small amounts of V. The T_S reaches 1000°C with the addition of just ~0.12 wt. pct. V, suggesting a limit of 0.1 wt. pct. V should be considered. THERMOCALC was used with a coherent M_2C model[3] to calculate the driving force for coherent M_2C carbide precipitation for all three compositions with and without 0.1 wt. pct. V, for increasing Cr. The results of these calculations are plotted in Figure 6. Without V, the driving force plot shows an optimum Cr level of 3-4 wt. pct. Cr. With the V addition the driving force increases several thousand J/mole and decreases linearly with increasing Cr. Addition of V was, therefore, justified by a substantial increase in driving force for carbide precipitation. The Cr level was maintained at 3 wt. pct. to allow full dissolution of cementite during M_2C precipitation. The M_S temperatures were recalculated for inclusion of V and found to change insignificantly.

In addition to maximizing the precipitation driving force, it is desirable to maximize the coarsening rate constant, K_C in order to minimize the degree of impurity

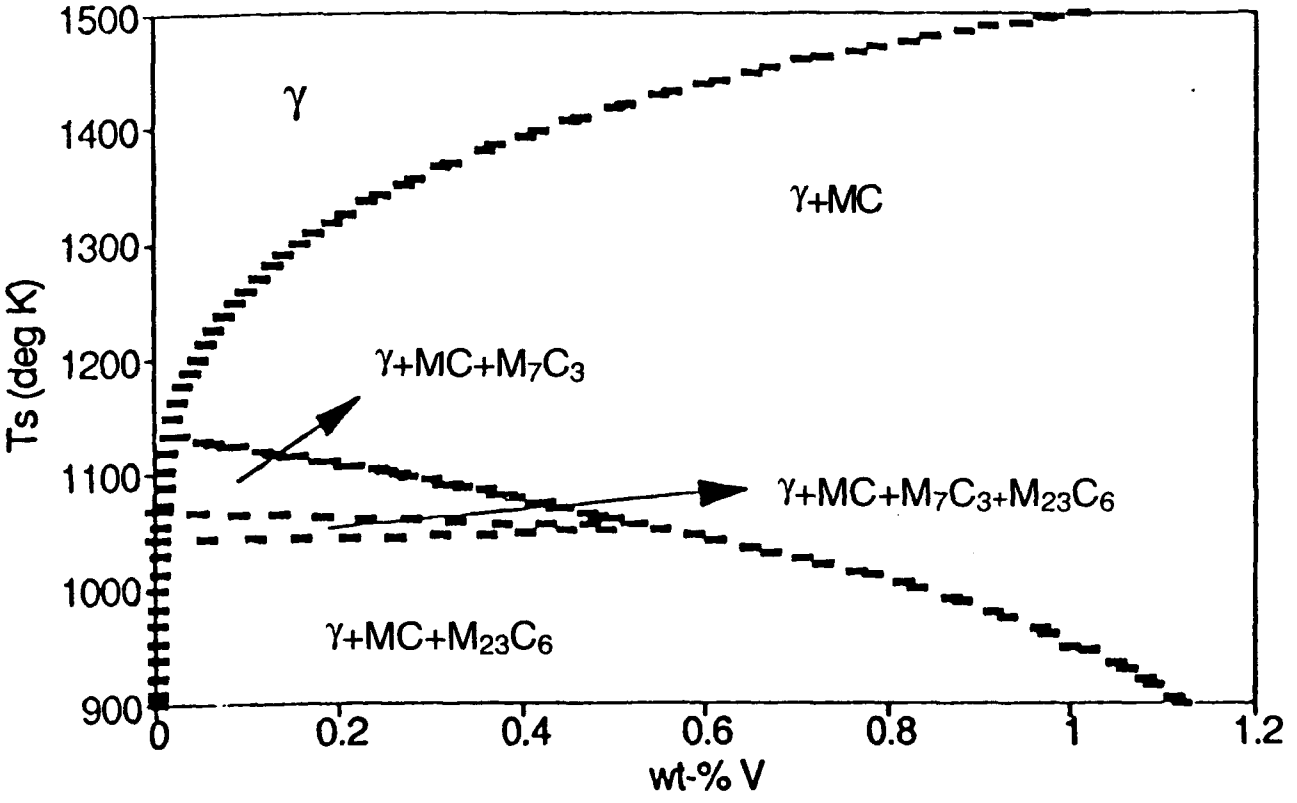

Figure 5. Phase diagram section vs. V content for Fe-13.5Co-10.6Ni-3Cr-1.1Mo-0.27C steels defining solution treatment conditions.

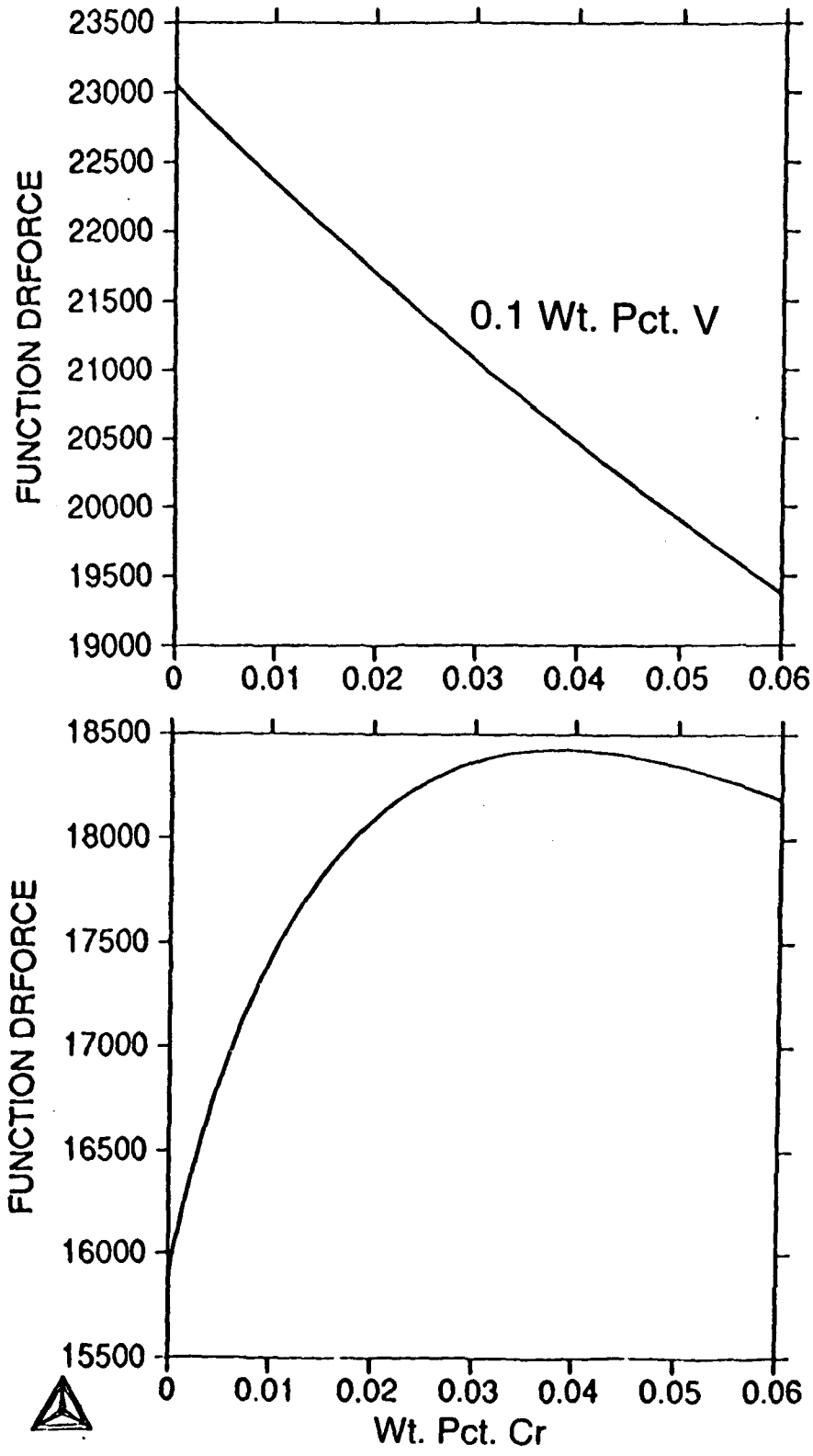

Figure 6. Coherent M_2C precipitation driving force at 500°C vs. content with (top) and without (bottom) 0.1V addition to Fe-13.5Co-10.6Ni-1.1Mo-0.27C.

segregation to grain boundaries during secondary hardening. From Figure 7 it can be seen that K_C increases in an approximately linear fashion with increasing Cr, without V. However, the addition of V causes K_C to drop one third its original value for the 3Cr alloys. This compromise is judged acceptable.

The final step in the design of this prototype steel was to check the effect of Cr on solution treatment temperature, which we wish to maintain below 1000°C (1273K). This was accomplished by computing phase diagram isopleths with respect to Cr, with and without 0.1V. Figure 8 shows that without V, the solution temperature increases strongly with Cr content. Figure 9 shows that the addition of 0.1V increases the solution temperature to just below 1273K, slightly decreasing with Cr content. The Cr-Mo levels were then maintained at the initial values of 3Cr-1.1Mo.

Based on the optimization of the design variables as described above, three prototype alloys were ordered:

MTL1: 12.5Co-10.2Ni-3Cr-1.1Mo-0.1V-0.27C

MTL2: 13.5Co-10.6Ni-3Cr-1.1Mo-0.1V-0.27C

MTL3: 14.5Co-10.9Ni-3Cr-1.1Mo-0.1V-0.27C.

To control impurities and grain-refining dispersions, Ti deoxidation and late rare-earth additions of La were specified. This is based on our previous identification[3] of Ti-based MC carbides as the best grain-refining dispersion in terms of resistance to microvoid nucleation, and La as an effective S getter in the absence of Mn. The alloys were prepared as 50 lb.VIM melts by Precision Castparts Corporation of Portland, Oregon. Melts were cast as 5" X 2" rectangular slabs, annealed at 675°C/16 hr., the hot top removed, and were grit blasted and spot ground. The slabs were shipped to Niagara Specialty Metals for hot rolling to 1/4" plate. The alloys were received with the following compositions:

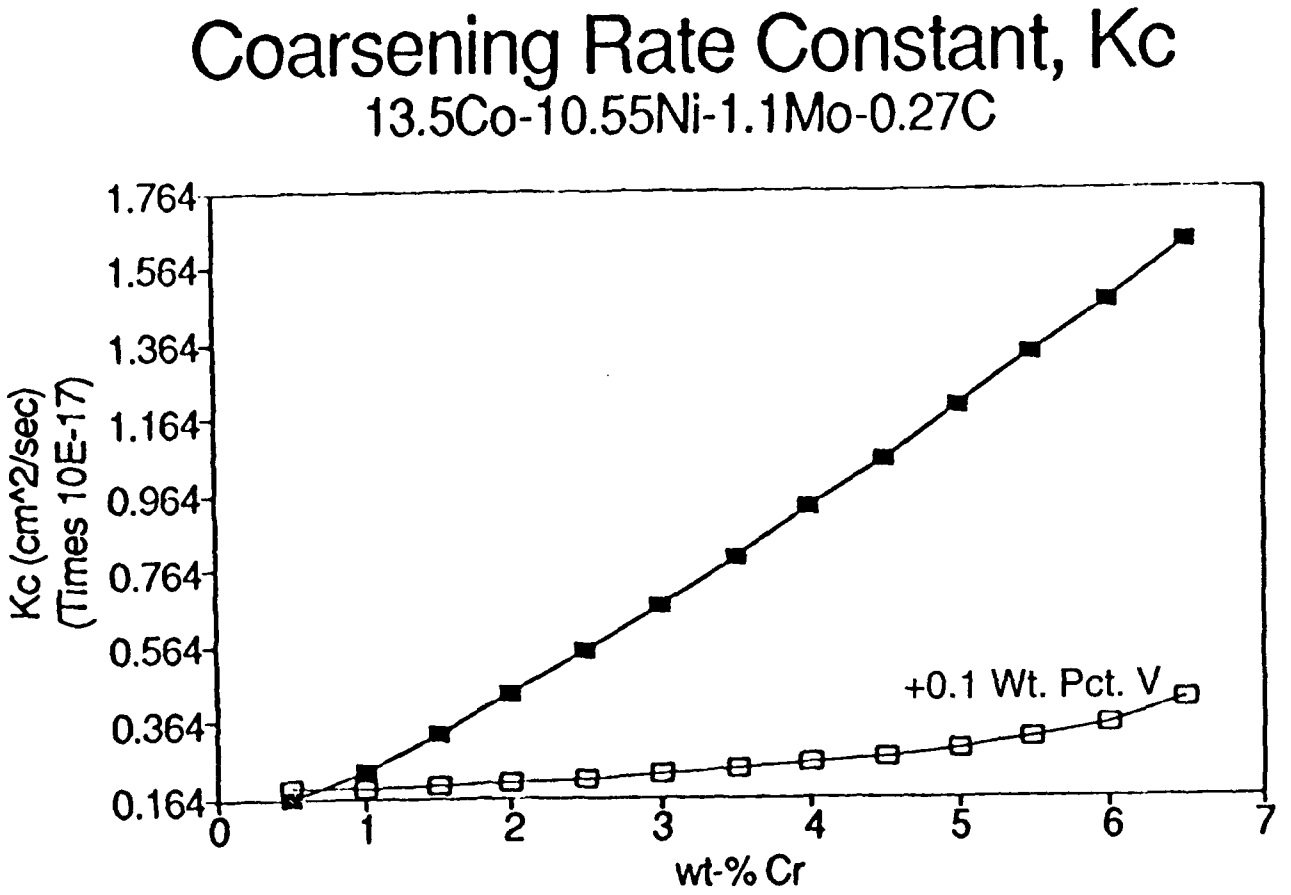

Figure 7. Computed M_2C coarsening rate constant at 500°C vs. Cr content with and without 0.1V.

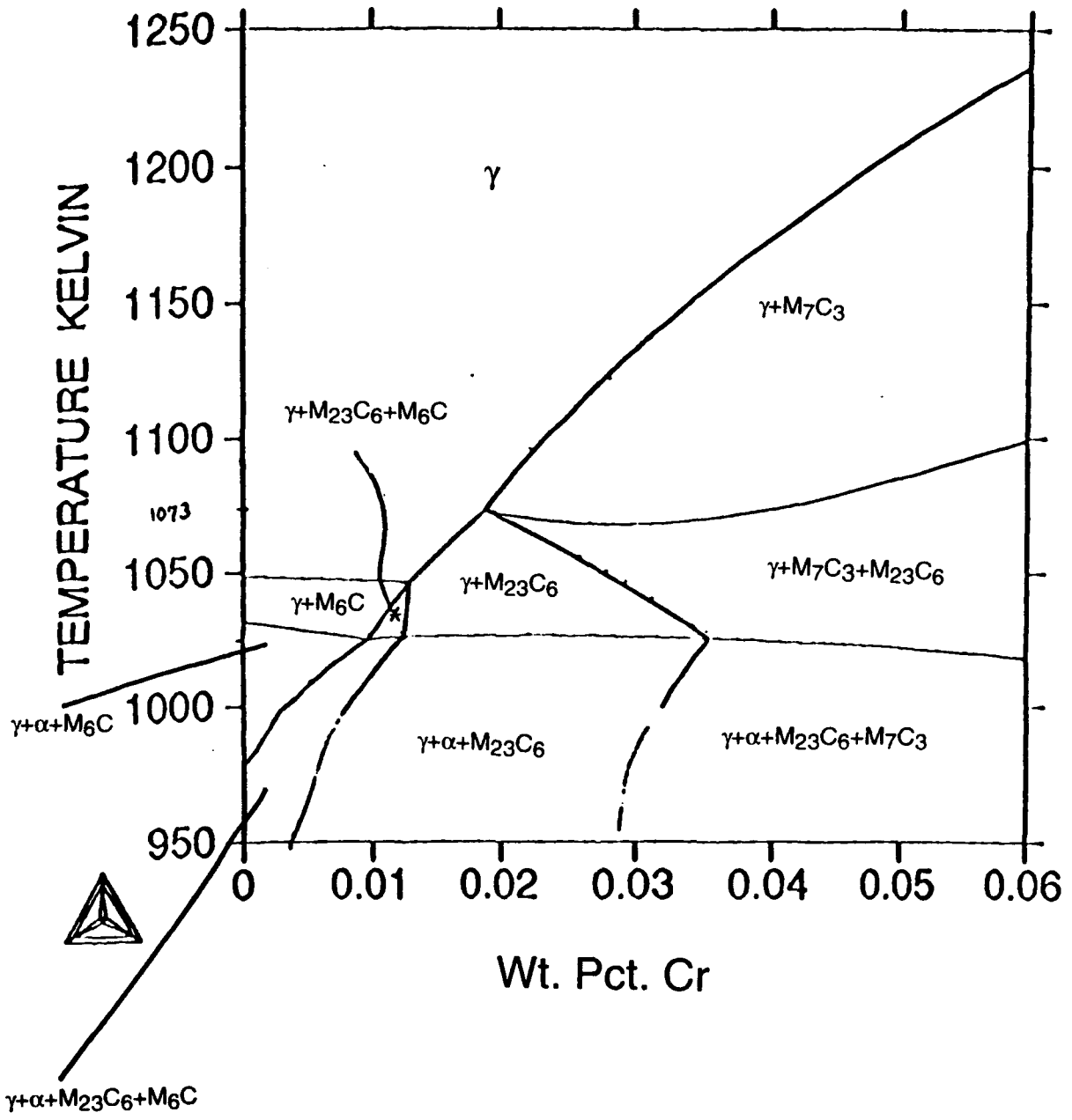

Figure 8. Phase diagram section vs. Cr content for Fe-13.5Co-10.6Ni-1.1Mo-0.27C.

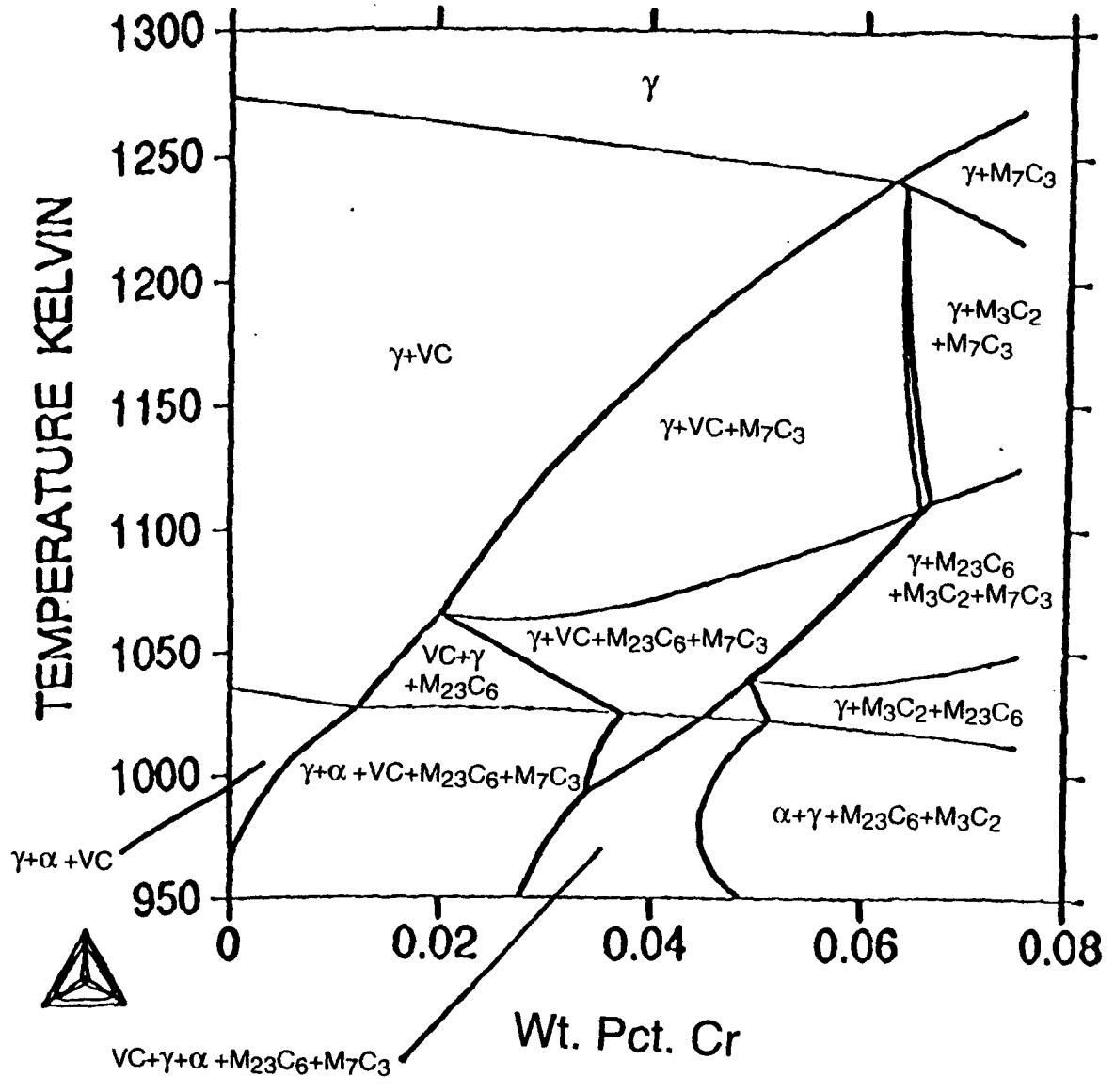

Figure 9. Phase diagram section vs. Cr content for system of Fig. 8 with addition of 0.1 V.

MTL1: 12.46Co-10.08Ni-2.92Cr-1.05Mo-0.095V-0.21C

MTL2: 13.45Co-10.59Ni-2.97Cr-1.15Mo-0.113V-0.30C

MTL3: 14.36Co-10.75Ni-2.94Cr-1.07Mo-0.1V-0.30C

Compositions were close to specifications with the notable exception of C content which was very low in MTL1 and slightly too high in MTL2 and MTL3. M_S temperatures were measured using a MMC computerized metallurgical quenching dilatometer. Initial measurements obtained by quenching from 1000°C provided elevated M_S temperatures, indicating that all the carbon may not have been in solution. The results shown in Table 1 were obtained by quenching from full solution treatment at 1200°C and are within ~20°C of model predictions. The M_S temperatures are suitable for obtaining desired lath martensitic structures, but the lower temperatures of the .30C alloys (MTL2 & 3) will tend to promote retained austenite.

TABLE 1

Martensite Start Temperatures

	Measured Ms(°C)+/- 2σ	Calculated Ms(°C)
MTL1	235 +/- 16	257
MTL2	201 +/- 19	220
MTL3	200 +/- 15	225

TESTING AND ANALYSIS

Central to our approach for enhancing fracture toughness in these martensitic steels is maintaining control of the M_2C carbide precipitation strengthening dispersion to eliminate competing carbide phases (and achieve a high strength level at minimum carbon content) while maintaining a fine MC carbide grain-refining dispersion during solution treatment. To assess the success of this approach in these alloys, TEM extraction replicas were made from alloy MTL3 to determine the distribution of undissolved carbides in size and composition. Two samples from alloy MTL3, one solution treated for 1 hr. at 1000°C and the other at 1100°C, and each tempered at 482°C for 10 hr. were replicated and examined by analytical electron microscopy. The larger carbides, on the order of 75nm in diameter, were infrequent and maintained compositions similar to those of the Xray fluorescence spectrum of Figure 10. These larger carbides were always Cr-rich, indicating an $M_{23}C_6$ (or possibly M_6C) carbide. The smaller carbides, on the order of 20nm in diameter, were much more frequent and maintained compositions similar to those in Figures 11 and 12. These compositions are indicative of the desired Ti-rich MC carbide. Although the larger carbides were apparent in the extraction replicas, their relative scarcity compared with the much more abundant small carbides indicates the dissolution of the coarse $M_{23}C6$ carbides was essentially complete during solution treatment. This leaves only the fine MC carbides as the microvoid-nucleation-resistant grain-refining dispersion[3].

K_{IC} fracture toughness tests were conducted in accordance with ASTM designation E399, "Standard Test Method for Plane Strain Fracture Toughness of Metallic Materials." Oversized blanks were wire-cut from plate, heat treated, then ground to the final 10mm x 5mm size. The fatigue crack starter notch was wire-cut after grinding so that the final crack plane orientation was L-S. Samples were pre-cracked in fatigue by loading in three-point bending. Plots of load vs. displacement were recorded

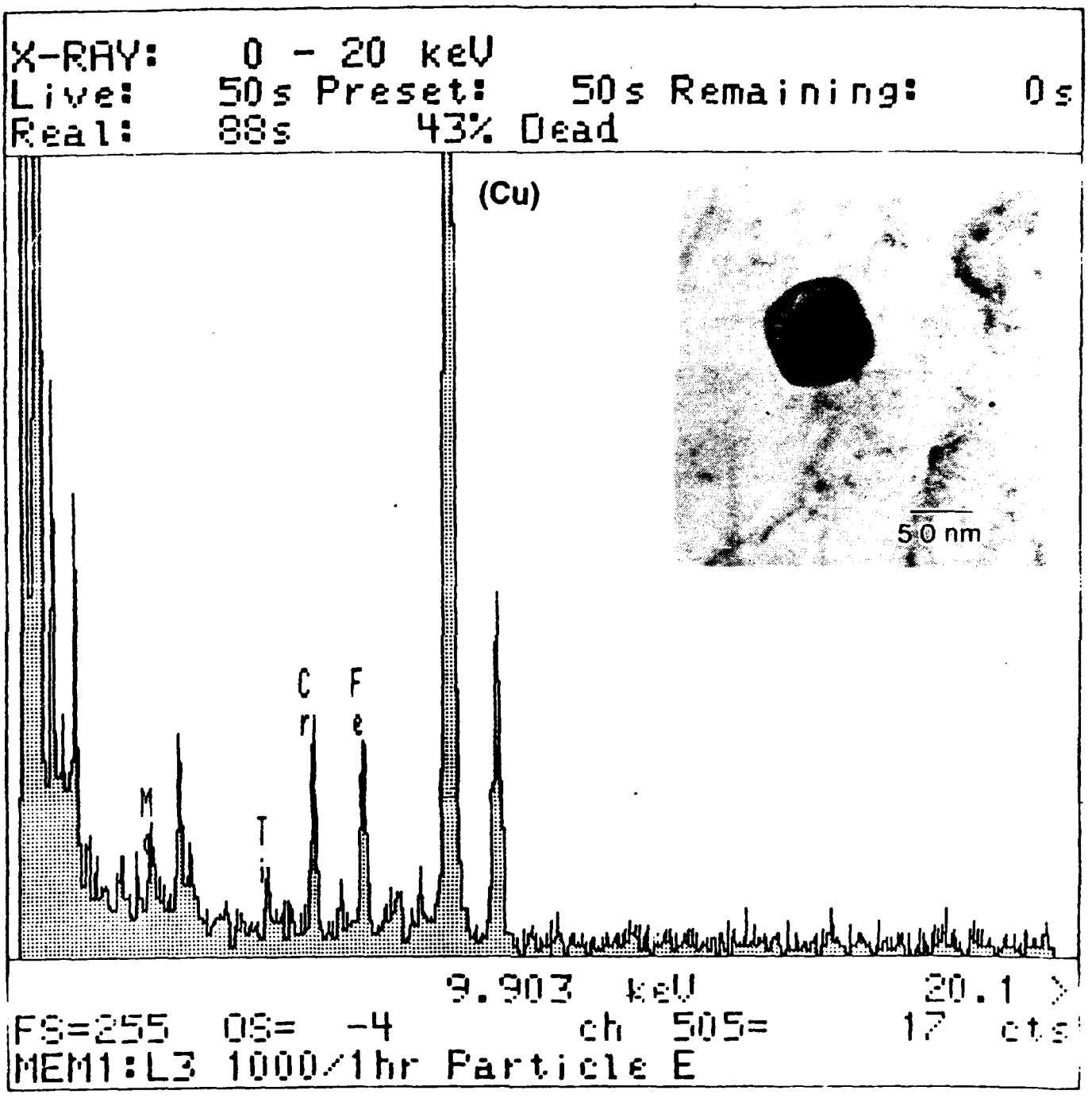

Figure 10. Energy dispersive X-ray spectrum from a large extracted carbide. High Cr content is indicative of a $M_{23}C_6$ or M_6C carbide. Cu signal is from specimen grid.

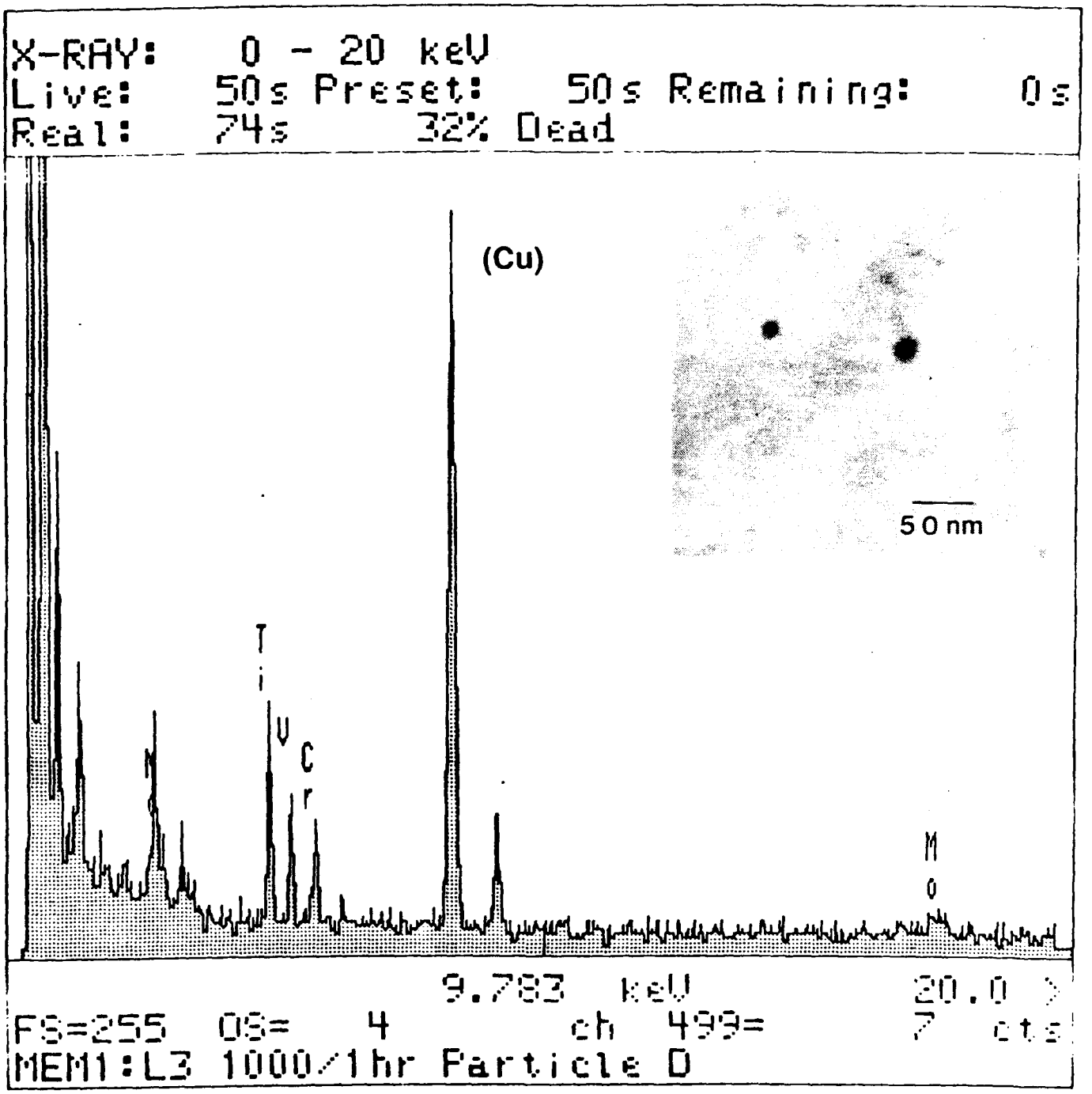

Figure 11. Energy dispersive X-ray spectrum from a small extracted carbide. The Ti, V, Mo Cr content is indicative of a MC carbide. Cu signal is from specimen grid.

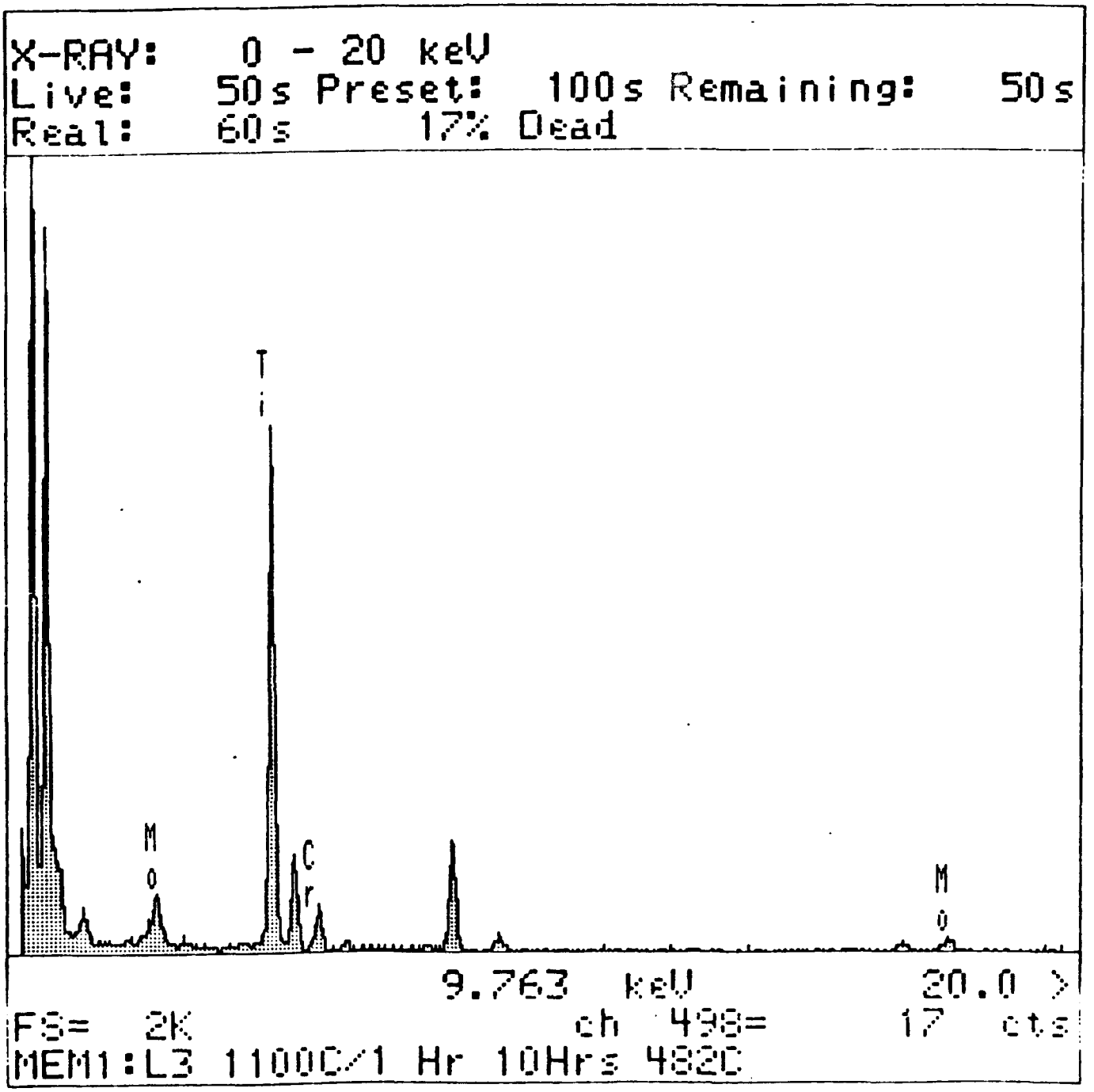

Figure 12. Energy dispersive X-ray spectrum from a small extracted carbide. The Ti, Mo, Cr content is indicative of a MC carbide.

for samples loaded to failure, and constructions were performed to calculate K_Q and to establish the validity of the K_{IC} measurement. To minimize cost, one sample was tested for each quoted K_{IC} measurement.

Figure 13 shows K_{IC} fracture toughness for alloys MTL1, MTL2 and MTL3 as a function of hardness after solution treatment at 1000°C for 1 hour and tempering for 0.5, 1, 5, 10 and 20 hr. at 482°C. The curve shapes suggest an optimal tempering time of ~8 hr. for the best strength/toughness combination, associated with near completion of cementite dissolution. Alloy MTL1 was fully solution treated at the 1000°C solution temperature as indicated by its high toughness; however, the lower carbon content, 0.21 weight percent compared to 0.30 for alloys MTL2 and MTL3, restricts its hardness to a maximum of RC 55.2. The higher carbon content in the other two alloys prevented complete solution treatment at 1000°C. The solution treatment study for alloys MTL2 and MTL3 was therefore extended to higher temperatures.

The effects of increasing solution treatment temperature together with an 8 hr. temper at 482°C on secondary hardening for alloys MTL2 and MTL3 are shown in Figures 14a and 14b, respectively. Here it can be seen that a hardness of RC 56.2 is attained for MTL2 at a solution treatment of 1100°C for 1 hr. Likewise, alloy MTL3 reaches a hardness peak of RC 56.4 at a solution treatment of 1125°C for 1 hr. The decreased hardness for higher solution temperatures is attributed to excessive retained austenite content. This is supported by an observed hardening effect of cyclic tempering with liquid nitrogen cooling. For solution treatment at 1100 to 1150C, saturation magnetization measurements indicate that the austenite content of MTL3 is 12-15pct after a conventional 8hr temper, and is reduced to 8-9pct by the cyclic tempering

Fracture toughness as a function of solution temperature for an 8 hr. temper at 482°C for alloys MTL2 and MTL3 are shown in Figure 14c. Peak toughness for alloy MTL2 is 69.4 ksi$\sqrt{in}$ attained at a solution treatment of 1100°C for 1 hr. while MTL3

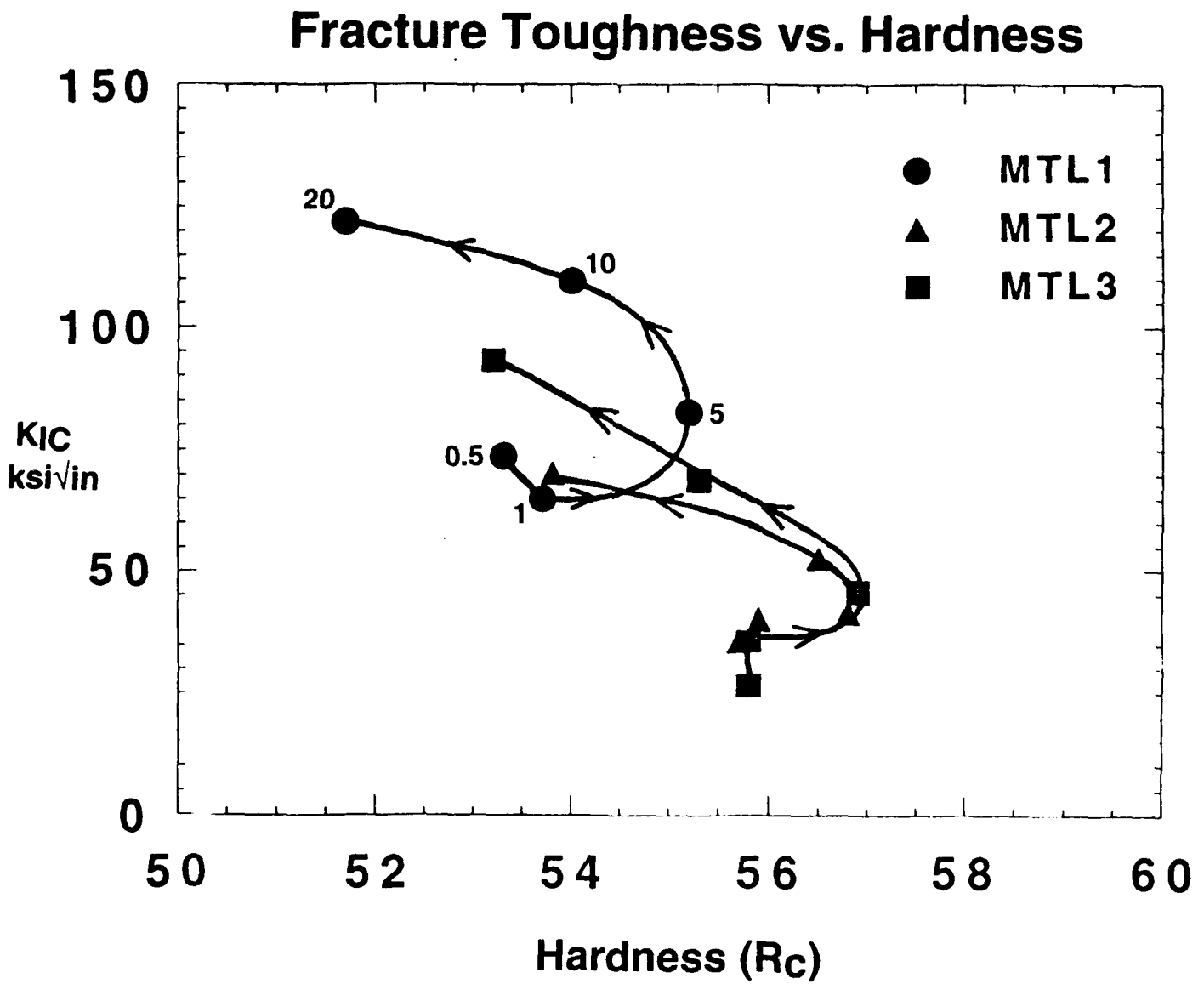

Figure 13. Measured toughness-hardness trajectory for the three prototype alloys for tempering at 482C after solution treatment at 1000C, 1 hr. Tempering times are 0.5, 1, 5, 10, and 20 hrs.

Hardness vs. Solution Temperature

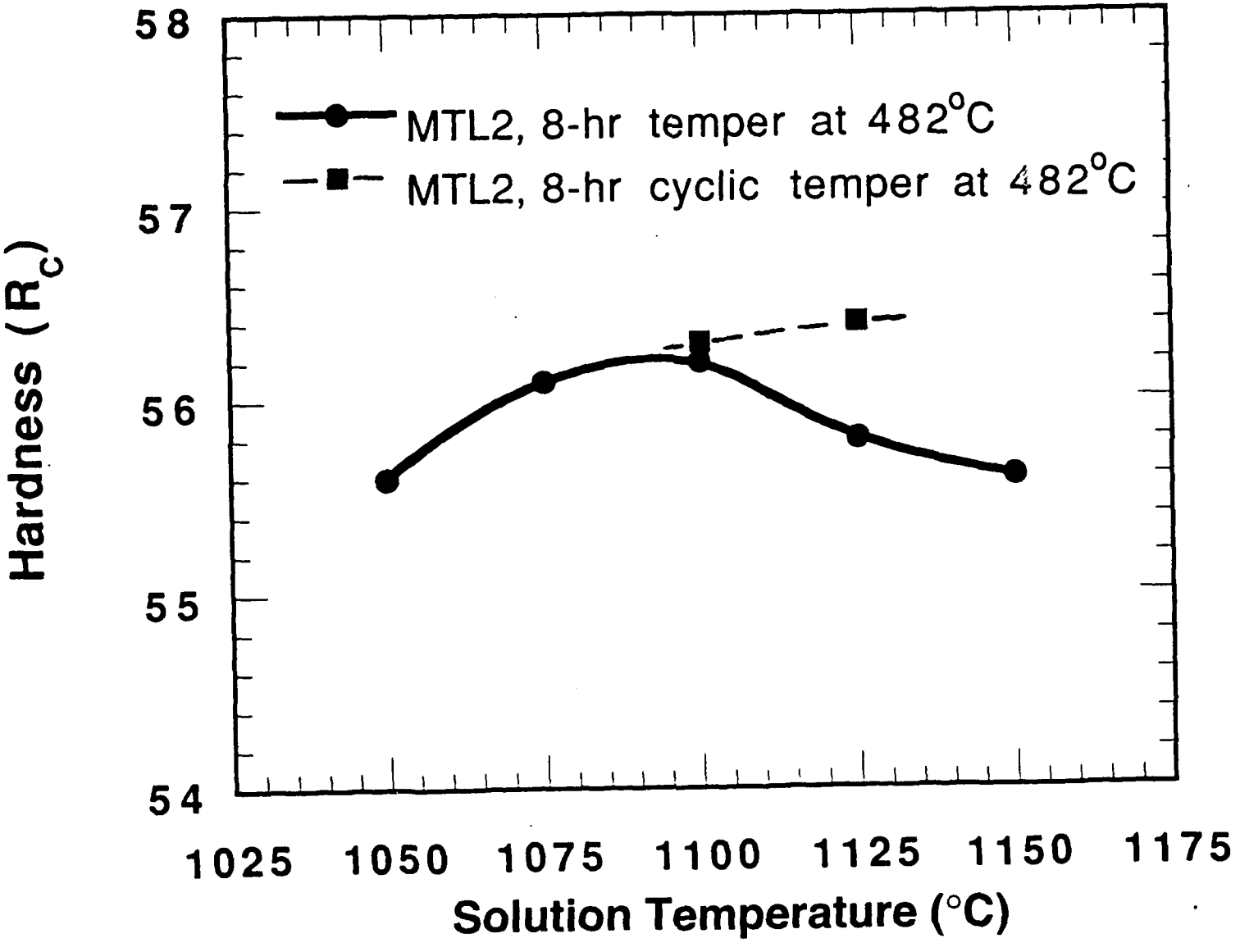

Figure 14a. Hardness vs. solution temperature (1 hr.) for MTL2 tempered 8 hr. at 482C. Cyclic tempering employed 2 hr. intervals.

Hardness vs. Solution Temperature

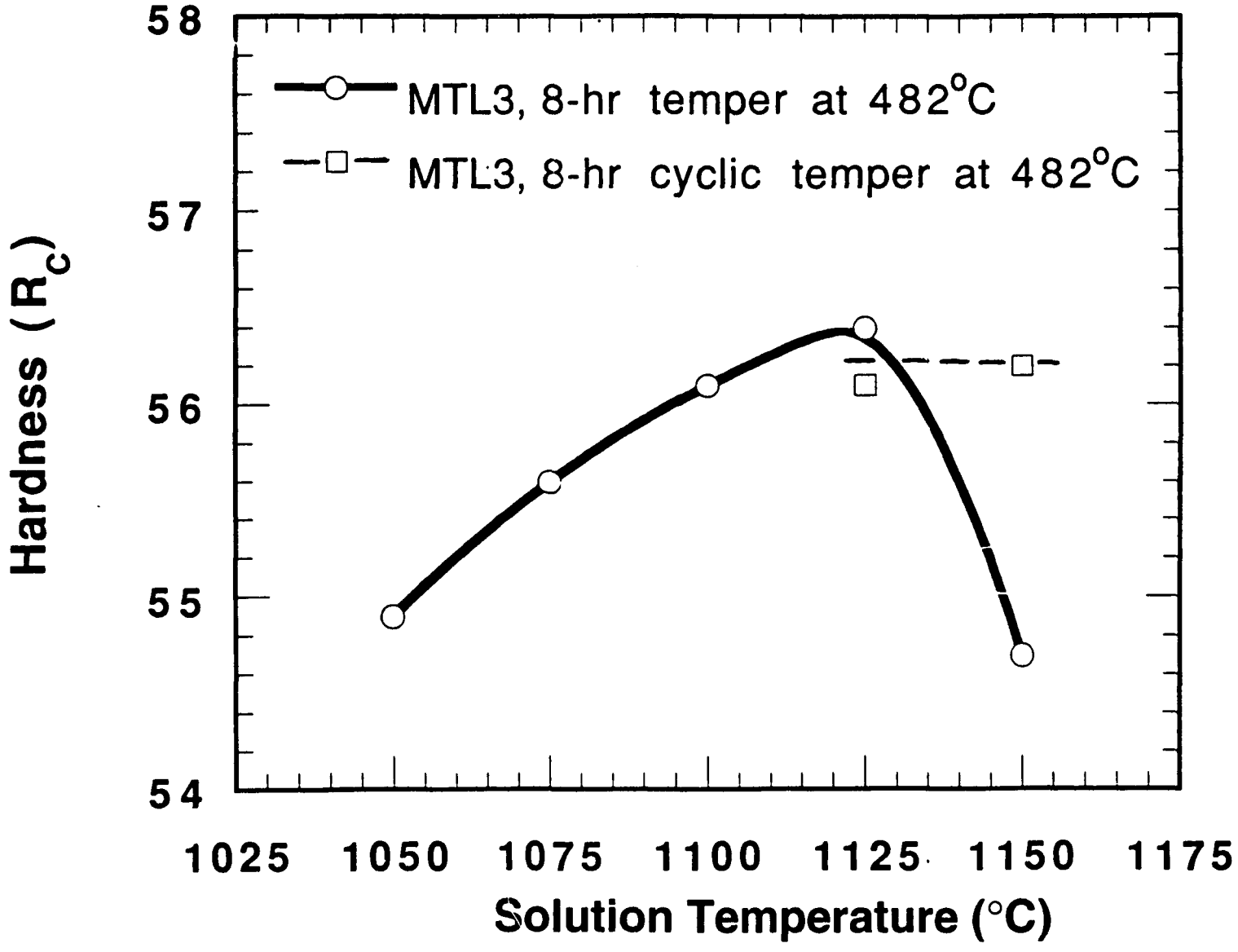

Figure 14b. Hardness as a function of solution treatment temperature together with an 8 hour temper at 482°C for alloy MTL3.

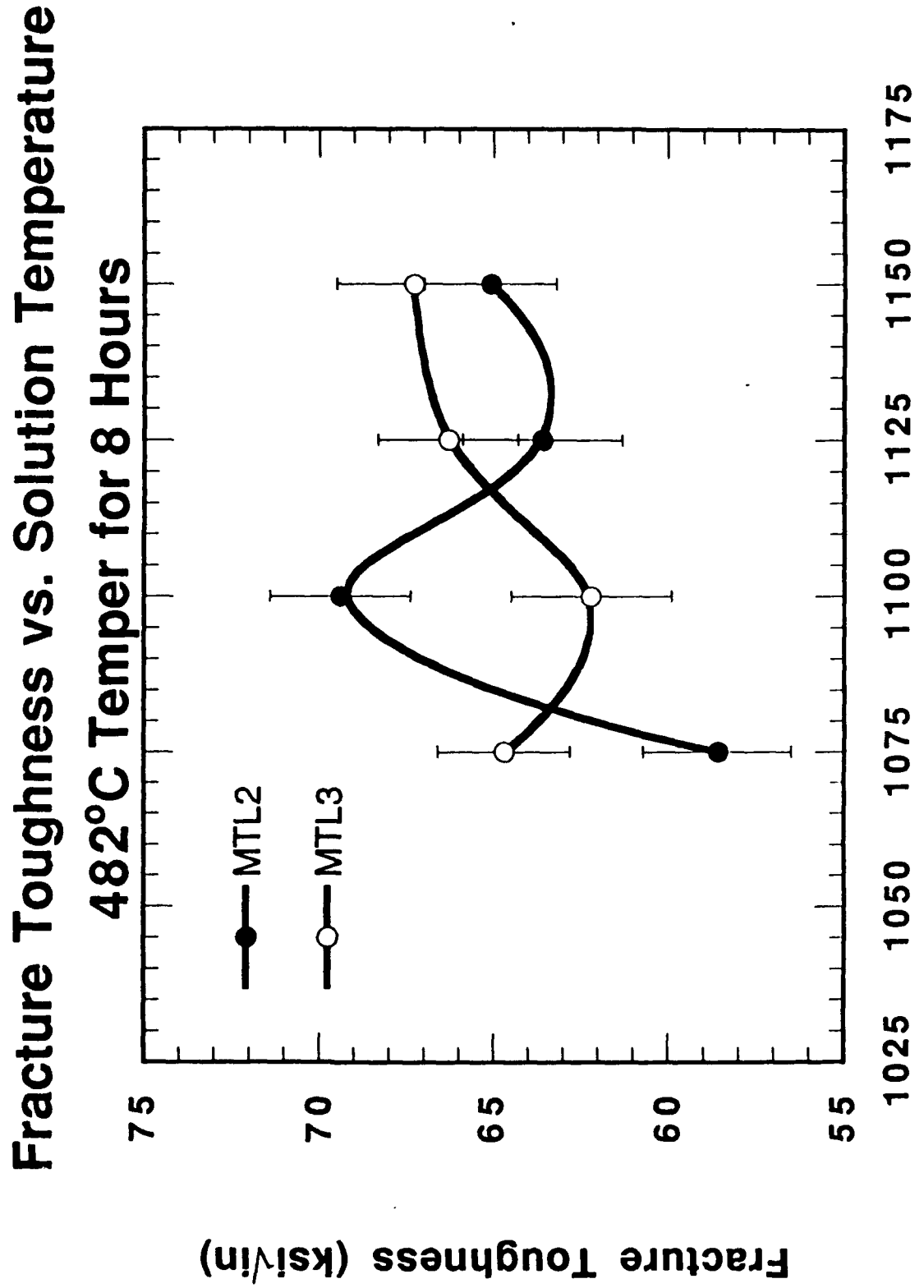

Figure 14c. K_{IC} toughness vs. solution temperature (1hr.) for MTL2 and MTL3 tempered 8hr. at 482C.

reaches 66.3 ksi$\sqrt{in}$ at 1125°C for 1 hr. Preliminary measurements using cyclic tempering on toughness at higher solution treatment temperatures shows no advantage in toughness.

A summary of the solution treatment study for alloys MTL2 and MTL3 is shown in Figures 15a and 15b, plotting fracture toughness/hardness combinations for increasing solution treatment temperatures, employing an 8 hr. temper at 482°C. Solution treatment condition TS2 represents the optimum heat treatment for alloy MTL2 (RC 56.2 at 69.4 ksi$\sqrt{in}$) in Figure 15a, while condition TS3 in Figure 15b is the optimum heat treatment for alloy MTL3 (RC 56.4 at 66.3 ksi$\sqrt{in}$). It is important to point out that this combination of high hardness and toughness was achieved without the benefits of transformation toughening that could be achievable with multi-step tempering in these compositions.

The hardness for MTL2 and MTL3 as a function of tempering time for cyclic tempering at 482°C for different solution treatment temperatures is shown in Figure 16. It is apparent that our 8 hr. temper is past peak hardness and represents the over-aged condition for both alloys MTL2 and MTL3. This condition is optimal for toughness, through dissolution of cementite by near-completion of M_2C alloy carbide precipitation.

It is important to further note that as solution treatment temperatures are increased, the alloys MTL2 and MTL3 begin to exhibit partial (~10%) intergranular fracture. Figure 17a-b are SEM micrographs of fracture surfaces taken from the K_{IC} plane strain fracture toughness tests. It is apparent from the faceting evident in the micrographs that some intergranular embrittlement has occurred. This may limit toughness under ballistic impact conditions, and could be improved in future heats by boron additions, to enhance grain boundary cohesion[3].

Figure 18 summarizes our recommended heat treatments for all three MTL alloys and compares their performance with our objectives on a plot of fracture toughness versus hardness. Although the property objectives are nearly attained, it is apparent that reducing the carbon content from 0.30 to 0.25 weight percent in alloys MTL2 and MTL3

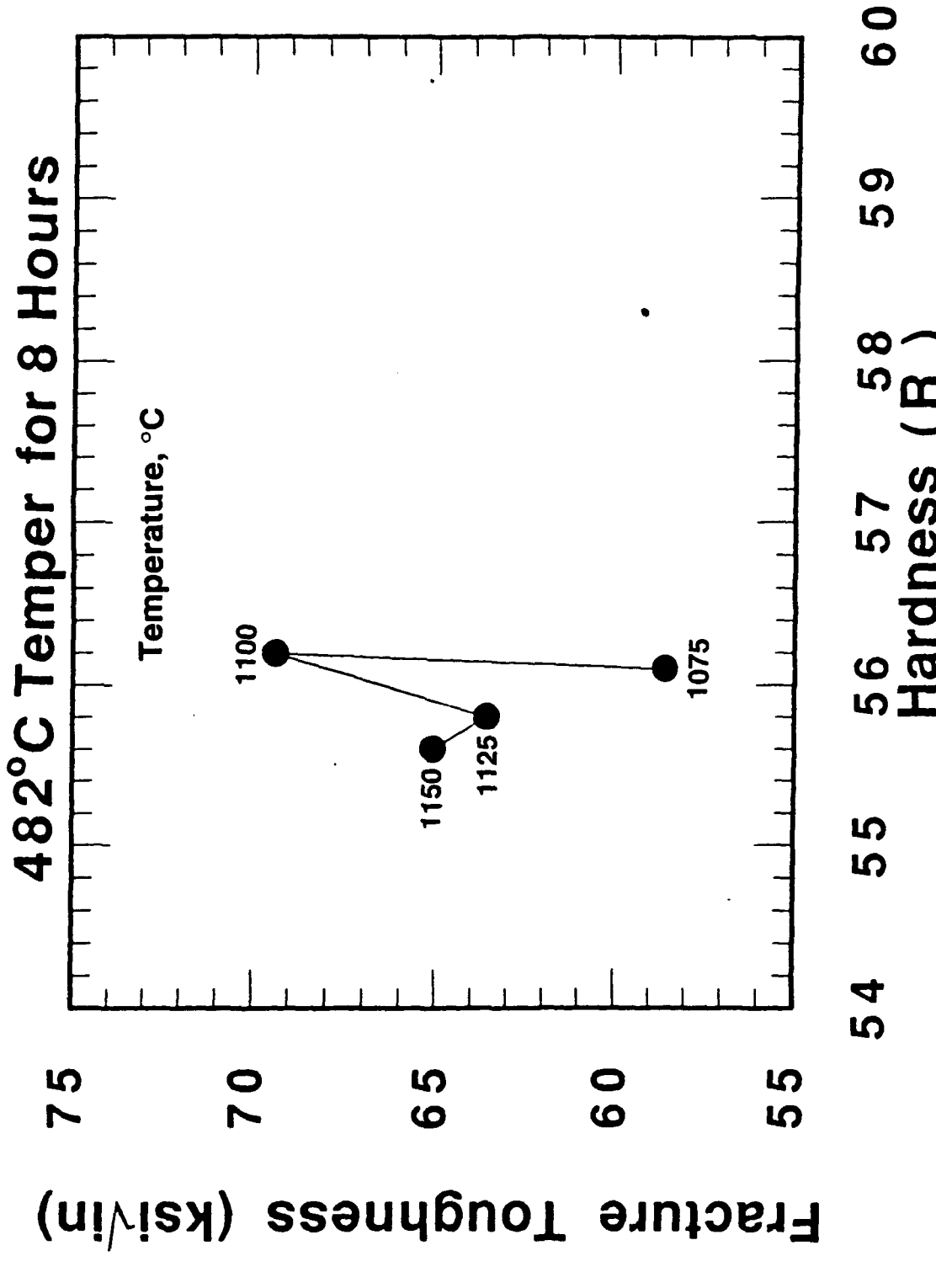

Figure 15a. Plane strain fracture toughness-hardness trajectory with increasing solution temperature for MTL2 tempered 8hr. at 482C.

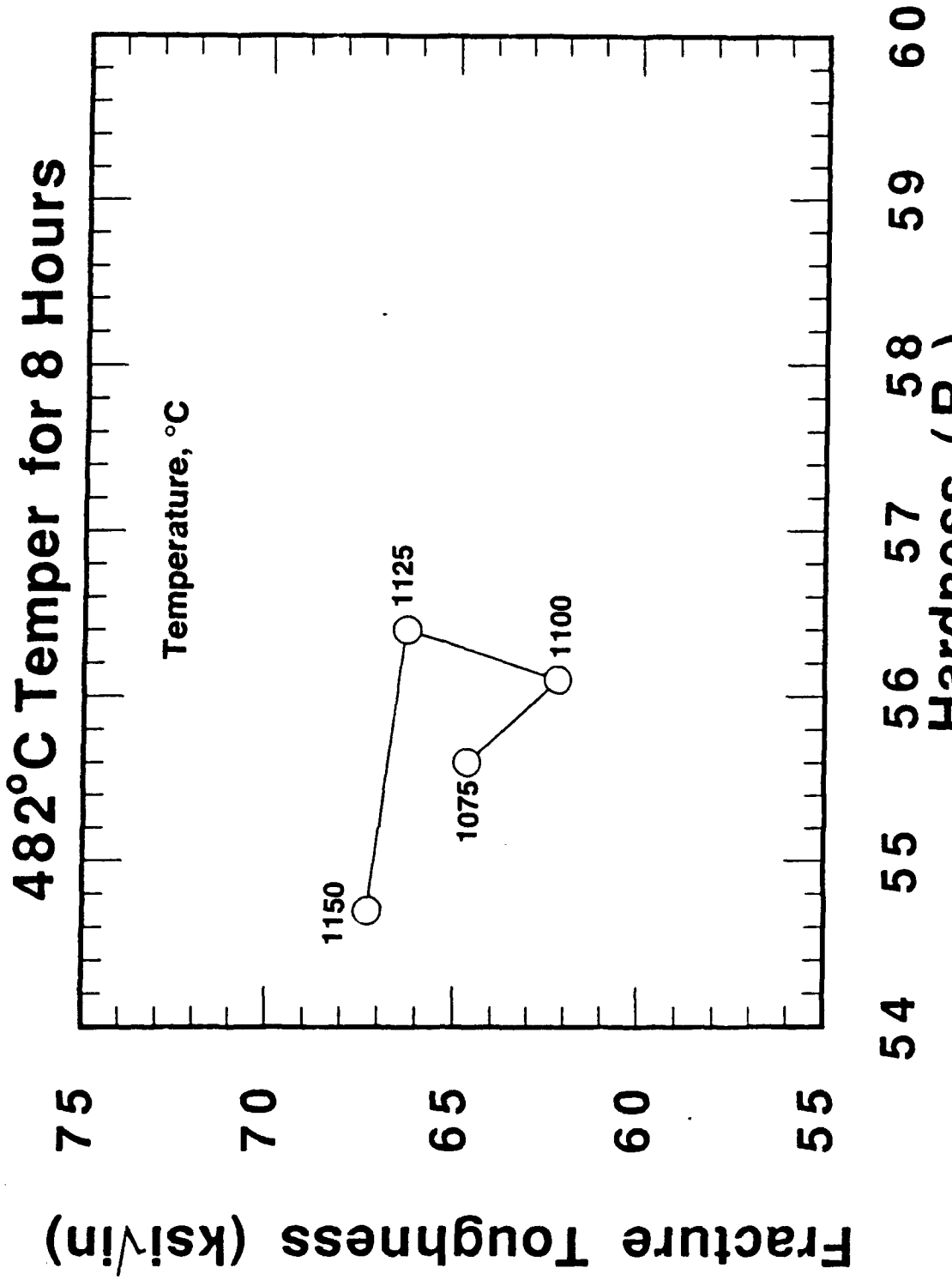

Figure 15b. Plane-strain fracture toughness-hardness trajectory with increasing solution temperature for MTL3 tempered 8hr. at 482C.

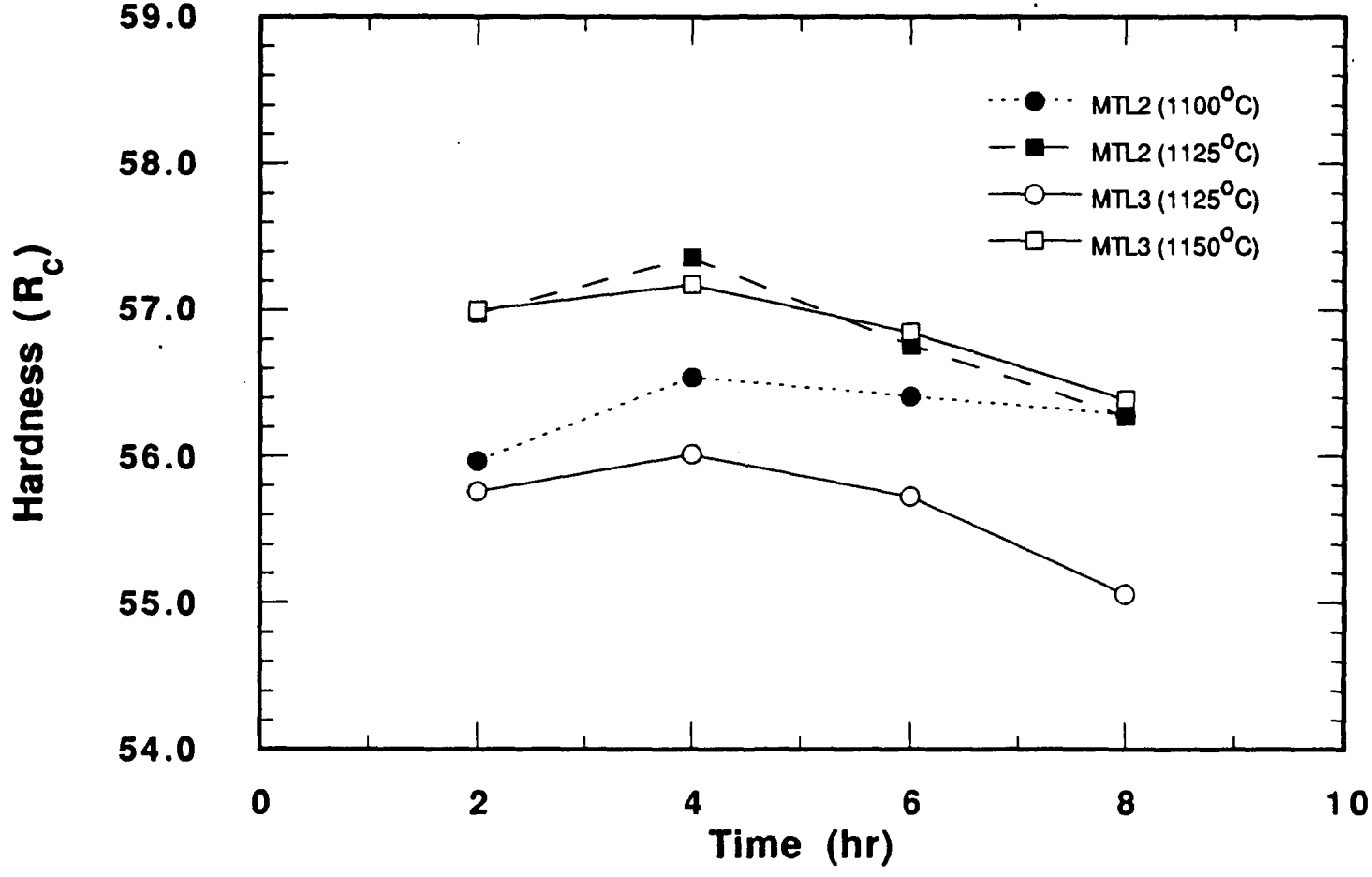

Figure 16. Hardness vs. cyclic tempering time with 2hr. intervals and liquid nitrogen cooling for the MTL2 and MTL3 alloys after high temperature solution treatments.

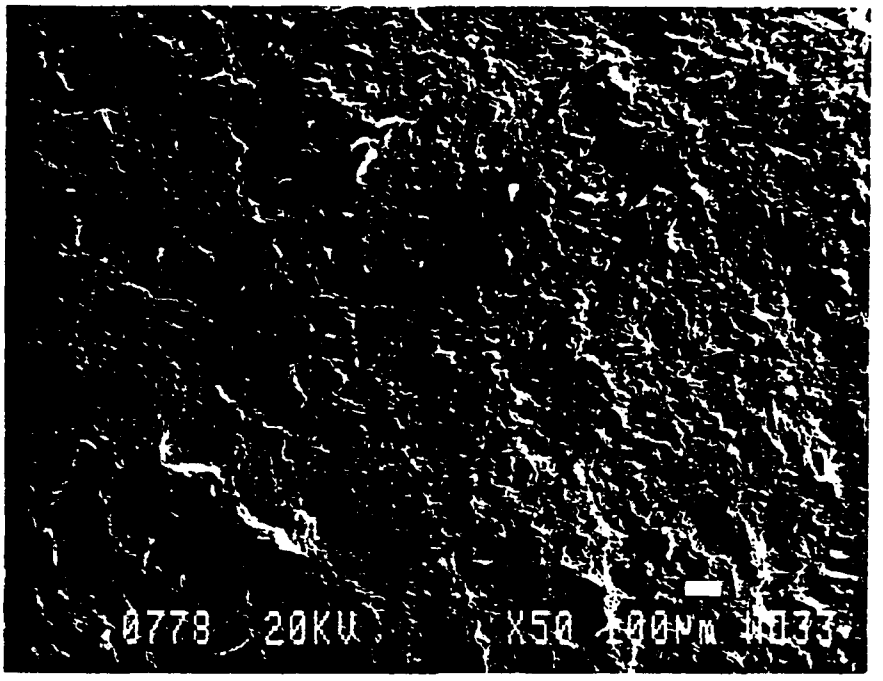

a) Alloy MTL2 solution treated at 1150°C for 1 hour followed with an 8 hour temper at 482°C.

b) Higher magnification view of alloy MTL2 solution treated at 1125°C for 1 hour followed with an 8 hour temper at 482°C.

Figure 17. SEM micrographs of fracture surfaces taken from K_{Ic} plain strain fracture toughness tests. Intergranular embrittlement is evident from the faceting.

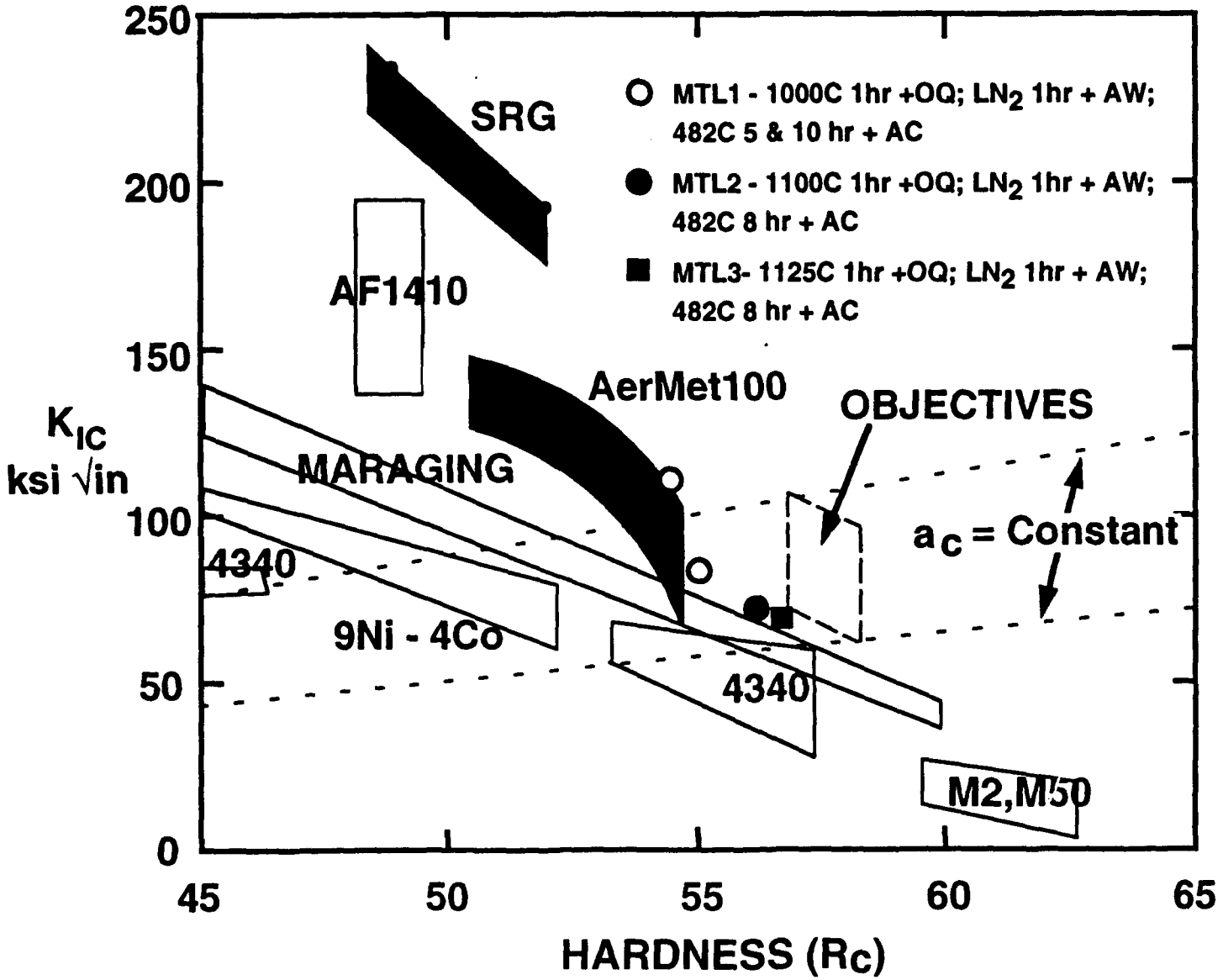

Figure 18. Summary of performance and recommended heat treatments for all three MTL alloys.

would increase toughness by reducing the solution treatment temperature and increase hardness by reducing retained austenite. Although the high solution temperatures required for MTL2 and 3 may promote quench cracking, the properties so far demonstrated appear worthy of ballistic testing. We thus recommend heat treatment of the available remaining plate material according to the conditions specified in Figure 18 for ballistic V_{50} measurements at ARL.

FURTHER DESIGN CALCULATIONS

The properties shown in Figure 18 demonstrate that the MTL1 composition matches the properties of Aermet 100 with only 0.21C compared to 0.24±.01C for the latter. This supports the predicted effectiveness of V in refining carbide size for strengthening efficiency. It is based on this result that we estimate that 0.25C should be sufficient to achieve the desired R_c57 hardness, provided the M_s temperature is kept sufficiently high (>220°C) to avoid excessive retained austenite.

Results of the first prototypes suggest that achieving our toughness objectives will require precipitated austenite transformation toughening which has not yet been demonstrated in the prototype alloys. Our further design calculations have addressed the further enhancement of transformation toughening potential.

The contour plot of toughening efficiency parameter (TEP) in Figure 4 suggests a desirable region in the upper left which is not accessible with Ni-Co variations alone due to M_s temperature limitations. The transformation dilatation model indicates that the additional degree of freedom necessary to access this level of TEP is best provided by variations in Cr content. Accordingly, Figure 19 plots the levels of austenite stability achievable in 3Cr and 4Cr modifications of MTL2 with Ni and Co adjusted to maintain an M_s temperature of 220C. The level of interest is denoted by that for the AF1410 steel where transformation toughening has been successfully demonstrated[2]. For the same alloys, Figure 20 plots the behavior of precipitated austenite fraction, transformation dilatation, and the toughness efficiency parameter (TEP). While the increased Cr level

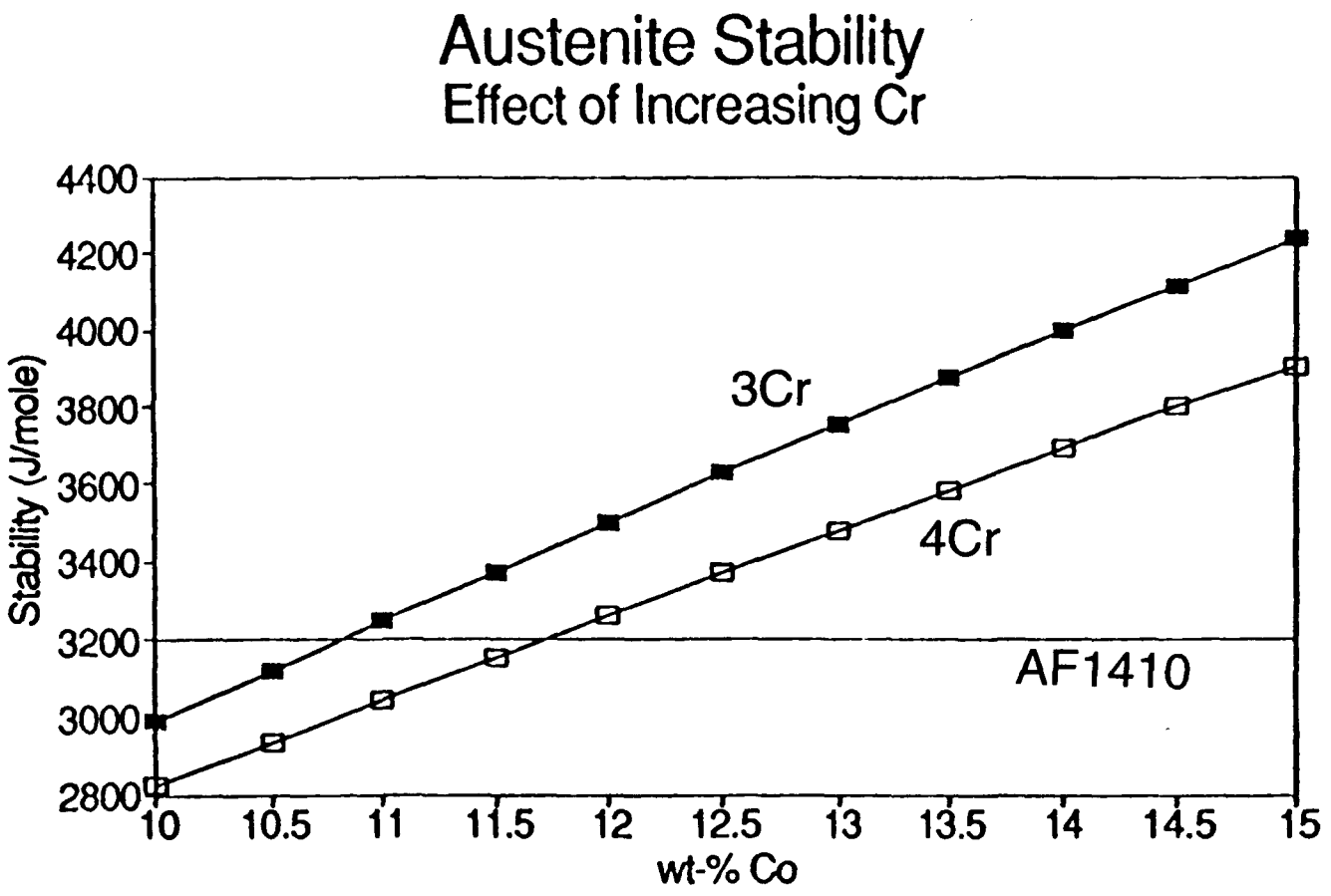

Figure 19. Stability of precipitated vs. wt. pct. Co. For 1.1Mo-0.27C-0.1V, studying the effect of increasing Cr from 3% to 4%.

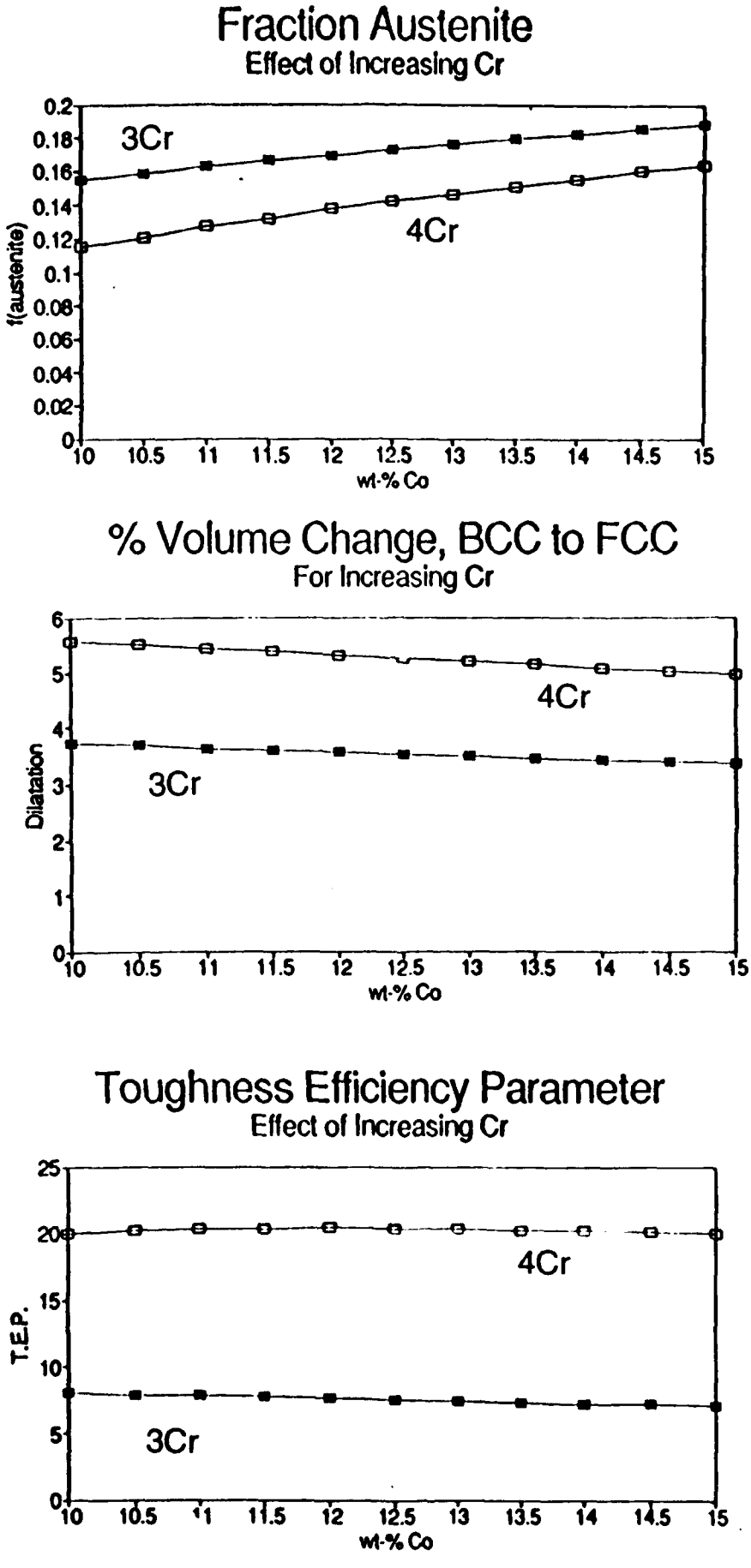

Figure 20. Precipitated austenite fraction, transformation dilatation, and toughening efficiency parameter (TEP) for alloy compositions of Fig. 19.

slightly decreases the austenite fraction, the dilatation is significantly increased such that the TEP is increased by a factor of 3. The phase diagram section of Figure 9 indicates that increasing Cr to this level causes no increase in solution temperature. Figure 7 indicates a negligible change in rate constant, and Figure 6 indicates a slight decrease in M_2C precipitation driving force. The higher Cr might, however, increase the stability of transient cementite.

Recent transformation toughening experiments[4] on Aermet 100 indicate that the faster M_2C precipitation kinetics in this alloy causes too much strength loss during austenite precipitation. Hence exploitation of precipitated austenite transformation toughening in the prototype armor steels may require slower carbide precipitation kinetics. This should be controllable through the predicted coarsening rate constant. However, slower tempering response would promote further impurity segregation at interfaces, tending to further promote intergranular fracture. It is anticipated that full exploitation of the transformation toughening potential of these alloys will require independent control of intergranular cohesion through gettering of embrittling impurities and addition of cohesion enhancers such as the boron mentioned earlier.

CONCLUSIONS AND RECOMMENDATIONS

Despite the problems associated with carbon contents outside of the specifications, the first prototype armor steels demonstrate the effectiveness of small V additions in achieving desired strength levels. With optimal solution treatments, 8 hr. tempering at 482°C gives strength/toughness combinations worthy of ballistic V_{50} tests on the remaining plate material. Optimal 1 hr. solution temperatures are 1000°C for MTL1, 1100°C for MTL2 and 1125°C for MTL3. The K_{IC} toughness of 69.4 ksi$\sqrt{in.}$ at R_C56.2 hardness may well be sufficient to resist plate shattering during ballistic impact, thus exploiting the greater ballistic performance potential of this hardness level.

Further design calculations suggest the potential for substantial transformation toughening in further modifications of these alloys, provided austenite and carbide precipitation kinetics can be suitably matched to avoid excessive softening, and intergranular cohesion can be suitably controlled.

REFERENCES

1. G. Ghosh and G. B. Olson, *Proc. Intl. Conf. Martensitic Transformations (ICOMAT-92)*, Monterey CA, July 19-24, 1992, in press.

2. G. N. Haidemenopoulos, G. B. Olson, and M. Cohen, "Dispersed-Phase Transformation Toughening in UHS Steels," in *Innovations in Ultrahigh-Strength Steel Technology*, eds. G. B. Olson, M. Azrin and E. S. Wright, Sagamore Army Materials Research Conf. Proc.: 34th (1990) 549-593.

3. G. B. Olson, "Overview: Science of Steel," in *Innovations in Ultrahigh-Strength Steel Technology*, eds. G. B. Olson, M. Azrin and E. S. Wright, Sagamore Army Materials Research Conf. Proc.: 34th (1990) 3-66.

4. C. J. Kuehmann, doctoral research in progress, Dept. Materials Science and Eng., Northwestern University, Evanston IL.

5. R. Wagner and R. Kampmann, "Solid State Precipitation at High Supersaturations", in *Innovations in Ultrahigh-Strength Steel Technology*, eds. G. B. Olson, M. Azrin and E. S. Wright, Sagamore Army Materials Research Conf. Proc.: 34th (1990) 209-222; J. S. Langer and A. J. Schwartz, *Phys. Rev. A21* (1980) 948.

APPENDIX

PROCESSING OF PROTOTYPE ARMOR STEELS

NORTHWESTERN UNIVERSITY
EVANSTON, ILLINOIS 60208-3116

STEEL RESEARCH GROUP
MATERIALS RESEARCH CENTER
2145 SHERIDAN ROAD

TELEPHONE: (708) 491-2847
FAX No.: (708) 491-7820

October 4, 1991

Dr. Xuan Nguyen-Dinh
Precision Cast Parts Corporation
4600 Southeast Harney Drive
Portland, OR 97206

Dear Dr. Nguyen-Dinh:

Following our phone conversation of November 8, 1991, the compositions of the 50 lb. VIM steel melts we would like to obtain are (wt. pct., bal. Fe):

	C	Co	Ni	Cr	Mo	V
MTL1	0.27	12.5	10.0	3.0	1.10	0.10
MTL2	0.27	13.5	10.4	3.0	1.10	0.10
MTL3	0.27	14.5	10.6	3.0	1.10	0.10

We would like the melts prepared from ultrahigh purity materials, keeping Mn and Si at <.01, and P and S at ~.001. Carpenter Steel is willing to contribute the high purity Fe (pharmaceutical grade "atomiron") if necessary. We would like the melts Ti deoxidized (final Ti .015 max) followed by La additions balanced to the P and S levels.

The melts should be cast as 5" x 2" slab, annealed at 1250F-16h, the hot top removed, followed by grit blasting and spot grinding. The slabs would then be shipped to Niagara Specialty Metals for hot rolling to 1/4" plate.

Depending on the cost, we may prefer to prepare MTL2 before the other two. Please give me an estimate at your earliest convenience, as we are anxious to prepare material for evaluation in a student Senior Project.

Please call me if you need further information.

Sincerely yours,

Gregory B. Olson

November 7, 1991

Processing for Northwestern University

I. Melting at Precision Cast Parts

VIM (high purity iron and alloys)
Cast 5" x 2" slab
Anneal 1250F (16h)
Remove hot top
Grit blast and spot grind

Precision Cast Parts Corp.
4600 S.E. Harney Dr.
Portland, OR 97206
Contact: Dr. Xuan Nguyen-Dinh
Telephone: (503) 652-4522

II. Rolling at Niagara

Slab size 5" x 2" (50 lbs.)
Hot Rolling (1800F)
Roll to 3/8" x 6" x length
A.C.
Anneal 1250F (16h)
Finish at .250" x 6" x length

Niagara Specialty Metals
12600 Clarence Center Road
Akeron, NY 14001
Contact: Lou Vallery, V.P.
(716) 542-5552

Heat Chemical Analysis (wt. pct.)

	MTL1	MTL2	MTL3
C	0.210	0.300	0.300
Co	12.46	13.45	14.36
Ni	10.08	10.59	10.75
Cr	2.92	2.97	2.94
Mo	1.05	1.15	1.07
V	0.095	0.113	0.10
Ti	0.0142	0.013	0.01
Al	0.001	0.001	0.001
Mn	0.04	0.04	0.04
Si	0.02		0.03
Cu	0.01	0.01	0.01
Cb	0.01	0.01	0.01
Ta	0.01	0.01	0.01
Sn	0.001		0.001
P	0.001		0.001
S	0.0001	<.001	<.001
N2	0.0001	0.0003	0.0003
O2	0.0038	0.0028	0.0010

DISTRIBUTION LIST

No. of Copies	To
1	Office of the Under Secretary of Defense for Research and Engineering, The Pentagon, Washington, DC 20301
	Director, U.S. Army Research Laboratory, 2800 Powder Mill Road, Adelphi, MD 20783-1197
1	ATTN: AMSRL-OP-SD-TP, Technical Publishing Branch
1	AMSRL-OP-SD-TA, Records Management
1	AMSRL-OP-SD-TL, Technical Library
	Commander, Defense Technical Information Center, Cameron Station, Building 5, 5010 Duke Street, Alexandria, VA 23304-6145
2	ATTN: DTIC-FDAC
1	MIA/CINDAS, Purdue University, 2595 Yeager Road, West Lafayette, IN 47905
	Commander, Army Research Office, P.O. Box 12211, Research Triangle Park, NC 27709-2211
1	ATTN: Information Processing Office
	Commander, U.S. Army Materiel Command, 5001 Eisenhower Avenue, Alexandria, VA 22333
1	ATTN: AMCSCI
	Commander, U.S. Army Materiel Systems Analysis Activity, Aberdeen Proving Ground, MD 21005
1	ATTN: AMXSY-MP, H. Cohen
	Commander, U.S. Army Missile Command, Redstone Arsenal, AL 35809
1	ATTN: AMSMI-RD-CS-R/Doc
	Commander, U.S. Army Armament, Munitions and Chemical Command, Dover, NJ 07801
1	ATTN: Technical Library
	Commander, U.S. Army Natick Research, Development and Engineering Center Natick, MA 01760-5010
1	ATTN: SATNC-MI, Technical Library
	Commasnder, U.S. Army Satellite Communications Agency, Fort Monmouth, NJ 07703
1	ATTN: Technical Document Center
	Commander, U.S. Army Tank-Automotive Command, Warren, MI 48397-5000
1	ATTN: AMSTA-ZSK
1	AMSTA-TSL, Technical Library
	President, Airborne, Electronics and Special Warfare Board, Fort Bragg, NC 28307
1	ATTN: Library
	Director, U.S. Army Research Laboratory, Weapons Technology, Aberdeen Proving Ground, MD 21005-5066
1	ATTN: AMSRL-WT

No. of Copies	To
	Commander, Dugway Proving Ground, UT 84022
1	ATTN: Technical Library, Technical Information Division
	Commander, U.S. Army Research Laboratory, 2800 Powder Mill Road, Adelphi, MD 20783
1	ATTN: AMSRL-SS
	Director, Benet Weapons Laboratory, LCWSL, USA AMCCOM, Watervliet, NY 12189
1	ATTN: AMSMC-LCB-TL
1	AMSMC-LCB-R
1	AMSMC-LCB-RM
1	AMSMC-LCB-RP
	Commander, U.S. Army Foreign Science and Technology Center, 220 7th Street, N.E., Charlottesville, VA 22901-5396
3	ATTN: AIFRTC, Applied Technologies Branch, Gerald Schlesinger
	Commander, U.S. Army Aeromedical Research Unit, P.O. Box 577, Fort Rucker, AL 36360
1	ATTN: Technical Library
	U.S. Army Aviation Training Library, Fort Rucker, AL 36360
1	ATTN: Building 5906-5907
	Commander, U.S. Army Agency for Aviation Safety, Fort Rucker, AL 3636
1	ATTN: Technical Library
	Commander, Clarke Engineer School Library, 3202 Nebraska Ave., N., Fort Leonard Wood, MO 65473-5000
1	ATTN: Library
	Commander, U.S. Army Engineer Waterways Experiment Station, P.O. Box 631, Vicksburg, MS 39180
1	ATTN: Research Center Library
	Commandant, U.S. Army Quartermaster School, Fort Lee, VA 23801
1	ATTN: Quartermaster School Library
	Naval Research Laboratory, Washington, DC 20375
1	ATTN: Code 6384
	Chief of Naval Research, Arlington, VA 22217
1	ATTN: Code 471
	Commander, U.S. Air Force Wright Research and Development Center, Wright-Patterson Air Force Base, OH 45433-6523
1	ATTN: WRDC/MLLP, M. Forney, Jr.
1	WRDC/MLBC, Mr. Stanley Schulman

No. of Copies	To
	U.S. Department of Commerce, National Institute of Standards and Technology, Gaithersburg, MD 20899
1	ATTN: Stephen M Hsu, Chief, Ceramics Division, Institute for Materials Science and Engineering
1	Committee on Marine Structures, Marine Board, National Research Council, 2101 Constitution Avenue, N.W., Washington, DC 20418
1	Materials Sciences Corporation, Suite 250, 500 Office Center Drive, Fort Washington, PA 19034
1	Charles Stark Draper Laboratory, 555 Technology Square, Cambridge, MA 02139
	Wyman-Gordon Company, Worcester, MA 01601
1	ATTN: Technical Library
	General Dynamics, Convair Aerospace Division, P.O. Box 748, Fort Worth, TX 76101
1	ATTN: Mfg. Engineering Technical Library
	Plastics Technical Evaluation Center, PLASTEC, ARDEC, Bldg. 355N, Picatinny Arsenal, NJ 07806-5000
1	ATTN: Harry Pebly
1	Department of the Army, Aerostructures Directorate, MS-266, U.S. Army Aviation R&T Activity - AVSCOM, Langley Research Center, Hampton, VA 23665-5225
1	NASA - Langley Research Center, Hampton, VA 23665-5255
	U.S. Army Vehicle Propulsion Directorate, NASA Lewis Research Center, 2100 Brookpark Road, Cleveland, OH 44135-3191
1	ATTN: AMSRL-VP
	Director, Defense Intelligence Agency, Washington, DC 20340-6053
1	ATTN: ODT-5A, Mr. Frank Jaeger
	U.S. Army Communications and Electronics Command, Fort Monmouth, NJ 07703
1	ATTN: Technical Library
	U.S. Army Research Laboratory, Electronic Power Sources Directorate, Fort Monmouth, NJ 07703
1	ATTN: Technical Library
1	Iqbal Shareef, Advanced Materials Technology Center, Caterpillar, Inc., P.O. Box 1875, Peoria, IL 61656-1875
1	Prof. H. Sehitoglu, 122 Latrobe Hall, John Hopkins University, Mechanical Engineering Dept., 3400 North Charles Street, Baltimore, MD 21218

No. of Copies	To
1	Dr. John Vitek, Oak Ridge National Laboratory, Bldg. 5500, MS 6376, P.O. Box 2008, Oak Ridge, TN 37831-6376
5	Prof. Gregory B. Olson, Materials Science and Engineering, 2030 Technological Institute, Northwestern University, Evanston, IL 60208-3108
	Director, U.S. Army Research Laboratory, Watertown, MA 02172-0001
2	ATTN: AMSRL-OP-WT-IS, Technical Library
1	AMSRL-OP-WT-IS, Visual Information Branch
1	AMSRL-PR-WT, Procurement
30	AMSRL-MA-CC, Morris Azrin COR